Evaluation of Irradiation Assisted Stress Corrosion Cracking and Void Swelling on Reactor Vessel Internals

Revision 0

Non-Proprietary

December 2014

REVISION HISTORY

Revision	Date	Page	Description
0	December 2014	All	First Issue

ABSTRACT

The Advanced Power Reactor 1400(APR1400) reactor vessel internals (RVI) consist of two major structures, referred to as the core support structures and internal structures. The core support structures are the structures or parts of structures that are designed to provide direct support or restraint of the core. Most of the components are made of stainless steel Type 304 and jointed by stainless steel Type [ ]TS.

It is well known that irradiation assisted stress corrosion cracking (IASCC) and void swelling (VS) are challenging degradation mechanisms affecting the integrity of the RVI. Therefore, it is required to assess the RVI of the APR1400 for these degradation mechanisms to show the maintenance of the RVI integrity during the design life of 60 years.

The evaluation has been mainly performed in accordance with the similar methodologies used for the screening assessments and functionality analyses by the EPRI. General description of the IASCC and VS evaluation approach is as follows:

1. RVI component lists of APR1400 are collected.
2. Initial screening is performed using the design values of fluences ($5x10^{19}$ n/cm^2).
3. Based on the result of step 2 above, evaluation scopes are determined for functionality assessment (radiation transport analysis, computational fluid dynamics (CFD) analysis and structural analysis).
4. Radiation transport analysis, CFD analysis, structural analysis are performed.
5. USERMAT module, which is developed by the EPRI, is used to identify the susceptibility to IASCC and VS of the RVI components.

The neutron fluences and heat source to which RVI components are to be exposed during the reactor operation are calculated using the monte carlo N-particle transport code(MCNP Code). ENDF/B-VII and ENDF/B-VI cross section libraries are used for neutron and gamma flux calculation, respectively. For this purpose, the conservative pin power distribution is used for the first 12 years (first 8 fuel cycles) and the best estimated and equilibrium power distributions are used for the remaining 48 year operation. Low-leakage fuel loading pattern is assumed.

Temperature and pressure distributions on the RVI components are determined using the CFD code, STAR-CCM+.

Effective stresses of the RVI components are calculated for the normal operating condition using ANSYS code. Temperature gradients and pressure distribution of the structures obtained by the CFD analysis are considered. For the welds, a residual tensile stress of 379.2 MPa (55 ksi) is applied.

To assess the effects of operating neutron fluences, temperatures and stresses on the material property changes and the susceptibility to IASCC and VS of RVI components, Usermat.f (USERMAT), ANSYS-based subroutine developed by EPRI, is used.

The assessment concludes that the effective stresses and volumetric changes of the components of the APR1400 RVI are below the IASCC susceptibility stress and [ ]TS volume %, respectively. IASCC susceptibility stress is calculated by the USERMAT. Therefore, the IASCC and VS do not affect the integrity of the APR1400 RVI during the 60 year design life.

TABLE OF CONTENTS

LIST OF TABLES

LIST OF FIGURES

ACRONYMS AND ABBREVIATIONS

APR	Advanced Power Reactor
BOC	beginning of cycle
CEA	control element assemblies
CFD	computational fluid dynamics
CS	core shroud
CSB	core support barrel
DPA	displacement per atom
EFPY	effective full power year
ENDF	evaluated nuclear data file
EOC	end of cycle
FAP	fuel alignment plate
FE	finite element
IASCC	irradiation assisted stress corrosion cracking
IBA	inner barrel assembly
ICI	in-core instrumentation
KHNP	Korea Hydro & Nuclear Power Co., Ltd.
LSS	lower support structure
MCNP Code	Monte Carlo N-Particle Transport Code
MOC	middle of cycle
MRP	material reliability program
NOP	normal operation
NRC	U.S. Nuclear Regulatory Commission
OD	outer diameter
RV	reactor vessel
RVI	reactor vessel internals
SV	state variable
VS	void swelling
UGS	upper guide structure
UGSSP	UGS support plate

Page intentionally blank

1 INTRODUCTION

The Advanced Power Reactor 1400(APR1400) reactor vessel internals (RVI) consist of two major structures, referred to as the core support structures and internal structures. They have the role to assure the integrity of the core by providing direct support, restraint, envelope for the core, etc. Most of the RVI components are made of stainless steel Type 304 and jointed by stainless steel Type 308L or 347 welds (Reference 1).

The RVI of the APR1400 operates in harsh conditions, such as long term exposure to neutron irradiation, high temperatures, reactor water environment, and other operating loads. Therefore, even though these internal structures are mainly made of Type 304 austenitic stainless steel, which is well known to have good mechanical and corrosion properties, these operating conditions, especially neutron irradiation, cause them to age, which aging is characterized by a chromium depletion along grain boundaries of austenitic stainless steel, decrease in ductility and fracture toughness of the steel, increase in yield and ultimate strength of the steel, and potential volume change due to void formation in the steel.

For these reasons, under certain conditions of stress, temperature, and level of irradiation (neutron fluence), irradiated stainless steels of the RVI may become susceptible to irradiation assisted stress corrosion cracking (IASCC), especially under high residual stress at the welding connections, which are one of the characteristics of the APR1400 RVI (Reference 2).

In addition, void swelling (VS) may appear at specific locations of the RVI due to high neutron fluence and high temperature under localized gamma heating and low velocity of coolant flow (Reference 2).

Recently, EPRI started research on aging management for pressurized water reactor internals and published several material reliability program (MRPs) to provide guidelines on the evaluation of aging and aging management methodologies and procedures for operating RVI, especially for reactors whose lives had been extended to 60 years (Reference 3, 4 and 5).

Even though the MRPs have the purpose of providing an evaluation or the management methodologies for operating RVI, similar evaluation methodologies can be applied to advanced but to-be-built or under construction nuclear power plants, such as the APR1400 fleet, in the design stage for the evaluation of neutron irradiation effects on their RVI design.

This report contains the evaluation results for the IASCC and VS susceptibility of the APR1400 RVI, which were obtained mainly based on the methodologies used for the screening analyses and functionality assessment by the EPRI.

2 DESCRIPTION OF THE APR1400 RVI

2.1 General Arrangement and Function of the Components (Reference 1)

The RVI are classified as the core support structures and internal structures. The core support structures are the structures or parts of structures that are designed to provide direct support or restraint of the core within the reactor vessel (RV). The internal structures are all structures within the RV other than the core support structures, fuel assemblies, control element assemblies (CEA) and instrumentation. The components of the RVI are divided into two major parts consisting of the core support barrel (CSB) assembly and the upper guide structure (UGS) assembly. The flow skirt, although functioning as an integral part of the coolant flow path, is separate from the RVI and is affixed to the bottom head of the RV. The general arrangement of the APR1400 reactor is as shown in Figure 2.1-1.

The major structural member of the RVI is the CSB assembly. The CSB assembly consists of the CSB, the lower support structure (LSS) and in-core instrumentation (ICI) nozzle assembly, and the core shroud. The CSB assembly is shown in Figure 2.1-2.

The CSB is a right circular cylinder including a heavy external ring flange at the top end and an internal ring flange at the lower end. The CSB is supported from a ledge on the RV. The CSB supports the LSS upon which the fuel assemblies rest. Shrunk-fit into the flange of the CSB are four alignment keys located 90 degrees apart. The RV closure head and flange, and the UGS assembly flange are slotted in locations corresponding to the alignment key locations to provide alignment between these components in the RV flange region. The upper section of the CSB contains two outlet nozzles that interface with internal projections on the RV outlet nozzles to minimize leakage of coolant from inlet to outlet. The weight of the CSB is supported at its upper end. Amplitude limiting devices, or snubbers, are installed on the outside of the CSB near the bottom end to limit the lateral movement of the core. The snubbers consist of six equally-spaced lugs around the circumference of the CSB. The lower flange of the CSB supports, secures and positions the LSS and is attached to the LSS by means of a welded flexural connection.

The LSS provides support for the core through the support beams and transmits the load to the CSB lower flange. The LSS and ICI nozzle assembly positions and supports the fuel assemblies, the core shroud, and the ICI nozzles. The structure is a welded assembly consisting of a short cylinder, support beams, a bottom plate, ICI nozzles and an ICI nozzle support plate. The LSS is made up of a short cylindrical section enclosing an assemblage of grid beams arranged in an egg-crate fashion. The outer ends of these beams are welded to the cylinder. The fuel assembly locating pins (hereafter called insert pins) are attached to the top of the beams. The insert pins in the beams provide orientation for the lower ends of the fuel assemblies. The bottoms of the main and secondary support beams are welded to the bottom plates which contain flow holes to provide proper flow distribution. These plates also provide support for the ICI nozzles, the support columns and the ICI nozzle support plate. The lower support structure and ICI nozzle assembly are shown in Figure 2.1-3.

The core shroud provides an envelope for the core and limits the amount of coolant bypass flow. The core shroud consists of a welded vertical assembly of plates designed to channel the coolant through the core. Circumferential rings and top and bottom end plates provide lateral support. The rings are attached to the vertical plates using the full length welded ribs and horizontal braces. A small gap is provided between the core shroud outer perimeter and the core support barrel in order to provide upward coolant flow in the annulus, which minimizes thermal stresses in the core shroud. The core shroud is shown in Figure 2.1-4.

The UGS assembly aligns and laterally supports the upper end of the fuel assemblies, maintains the CEA spacing, holds down the fuel assemblies during operation, prevents fuel assemblies from being lifted out of position during a severe accident condition and protects the CEA from the effects of coolant cross flow

in the upper plenum. The UGS assembly consists of the UGS barrel assembly and the inner barrel assembly (IBA) (Figure 2.1-5).

The UGS barrel assembly consists of the UGS support barrel, fuel alignment plate (FAP), the UGS support plate, and CEA guide tubes. The UGS support barrel consists of a right circular cylinder welded to a ring flange at the upper end and to a circular plate (UGS support plate) at the lower end. The flange, which is a supporting member for the entire UGS assembly, sits on its upper side against the RV head during operation. The lower side of the flange is supported by the holddown ring, which sits on the CSB upper flange. The UGS flange and the holddown ring engage the CSB alignment keys by means of four accurately machined and located keyways equally spaced at 90 degree intervals. This system of keys and slots provides an accurate means of aligning the core with the closure head and thereby with the CEA drive mechanisms. The FAP is positioned below the UGS support plate by cylindrical CEA guide tubes. These tubes are attached to the UGS support plate and the FAP. The FAP is designed to align the lower ends of the CEA guide and insert tubes that in turn locate the upper ends of the fuel assemblies. The FAP also has four equally spaced slots on its outer edge that engage with lugs protruding from the core shroud to provide alignment. The CEA guide and insert tubes bear the upward force on the fuel assembly holddown devices. This force is transmitted from the FAP through the CEA guide tubes to the UGS barrel support plate.

The IBA limits cross flow and provides separation of the CEA. The IBA consists of a top plate welded to a right circular barrel open at the bottom and containing an assemblage of large vertical tubes connected by vertical plates in a grid pattern welded to the inside of the barrel. The IBA is held in position by continuous weld between the barrel flange and the top surface of the UGS barrel upper flange. Guides for the CEA extension shafts are provided by the top plate of the IBA. The tubes and connecting plates within the IBA are furnished with multiple holes to permit hydraulic communication.

The main coolant from the four RV inlet nozzles flows down to the flow skirt through the annulus between the RV and the CSB and flows upward through the core support region and the reactor core. Finally it exits through two reactor outlet nozzles. A portion of this flow bypasses to cool the RVI and the CEA. The reactor coolant flow path is depicted in Figure 2.1-6.

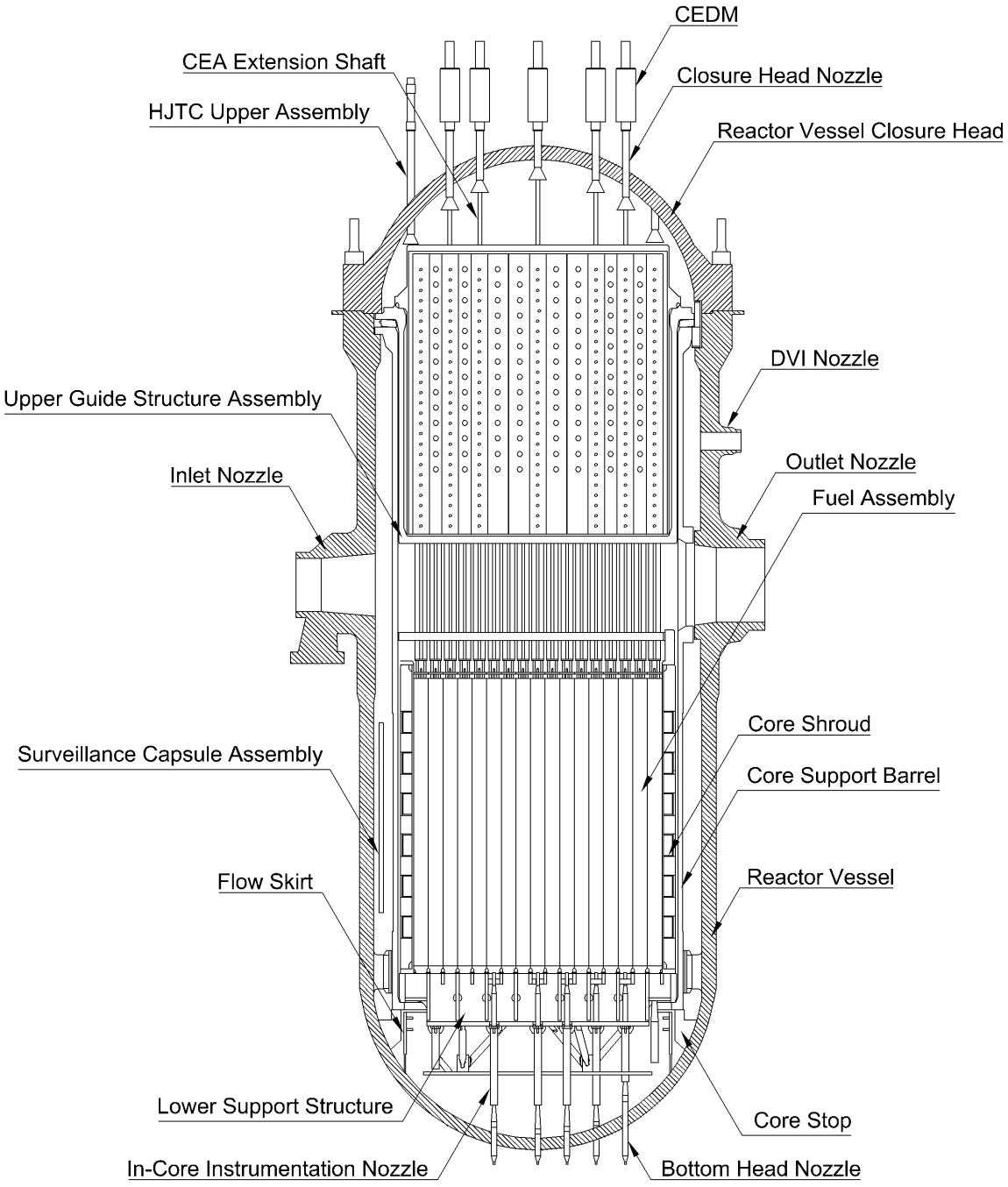

Figure 2.1-1 General Arrangement of the RVI

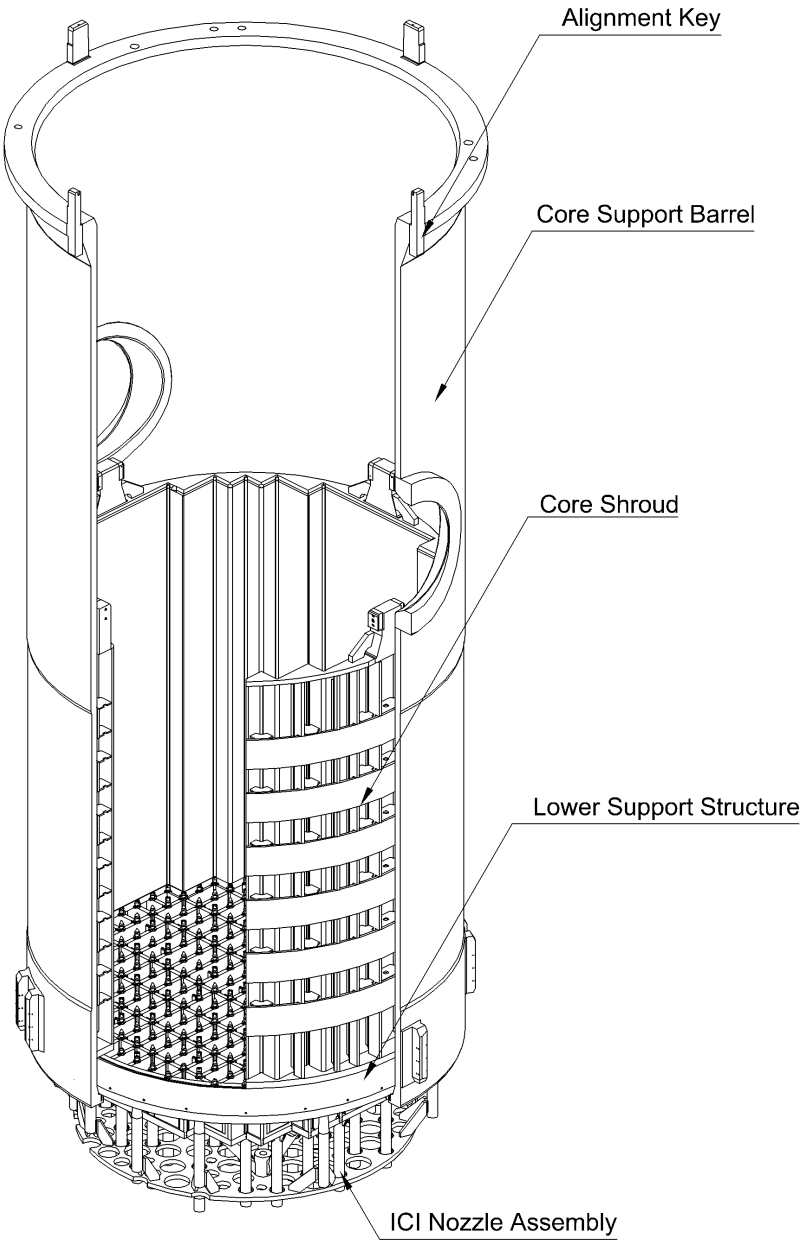

Figure 2.1-2 CSB Assembly

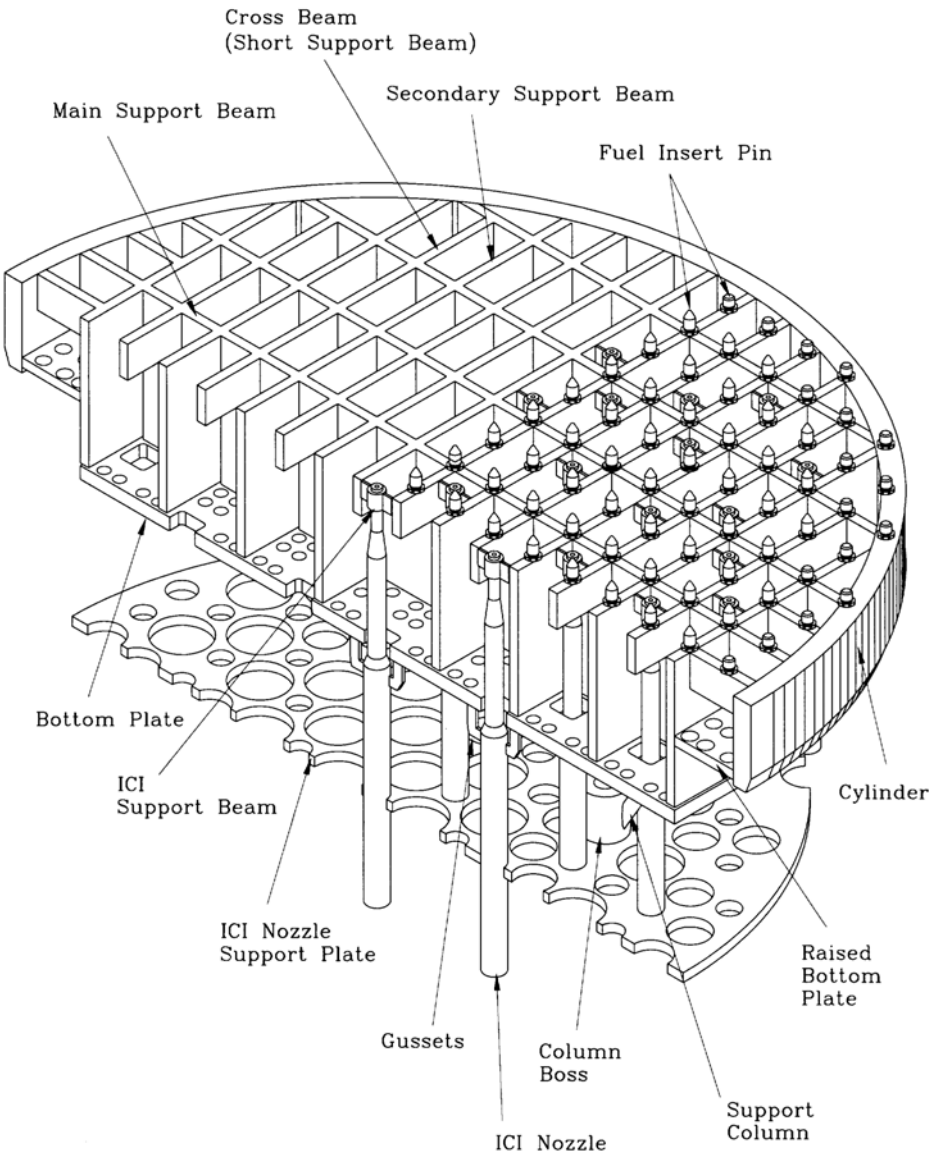

Figure 2.1-3 Lower Support Structure (LSS) / ICI Nozzle Assembly

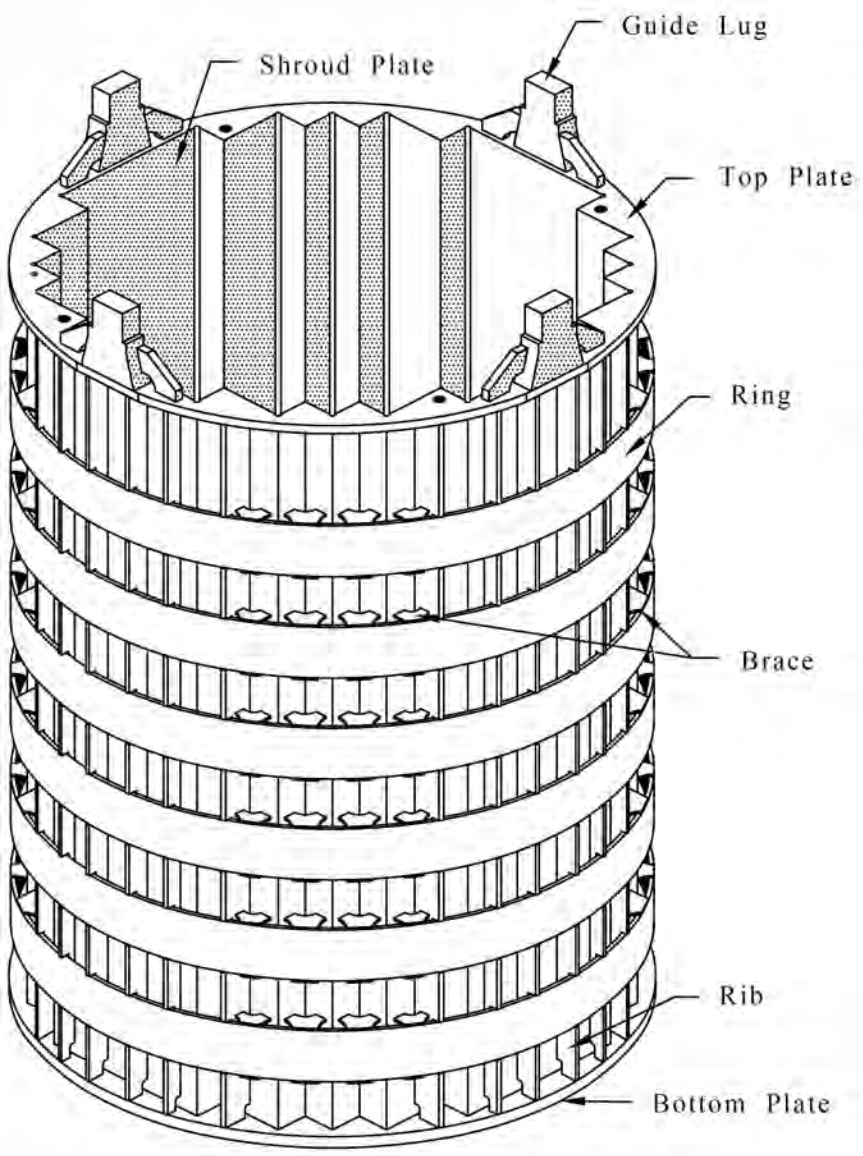

Figure 2.1-4 Core Shroud (CS)

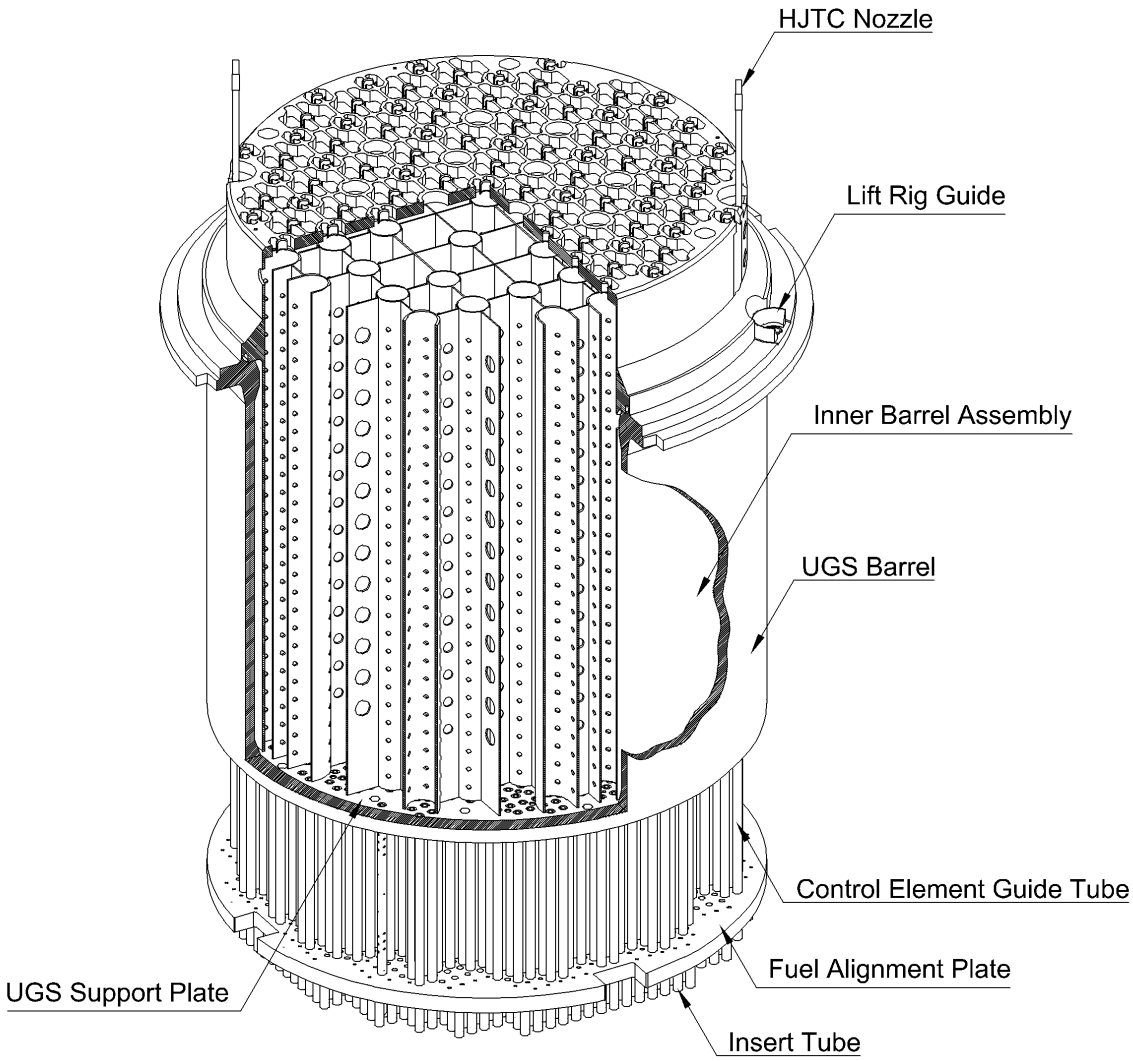

Figure 2.1-5 UGS Assembly

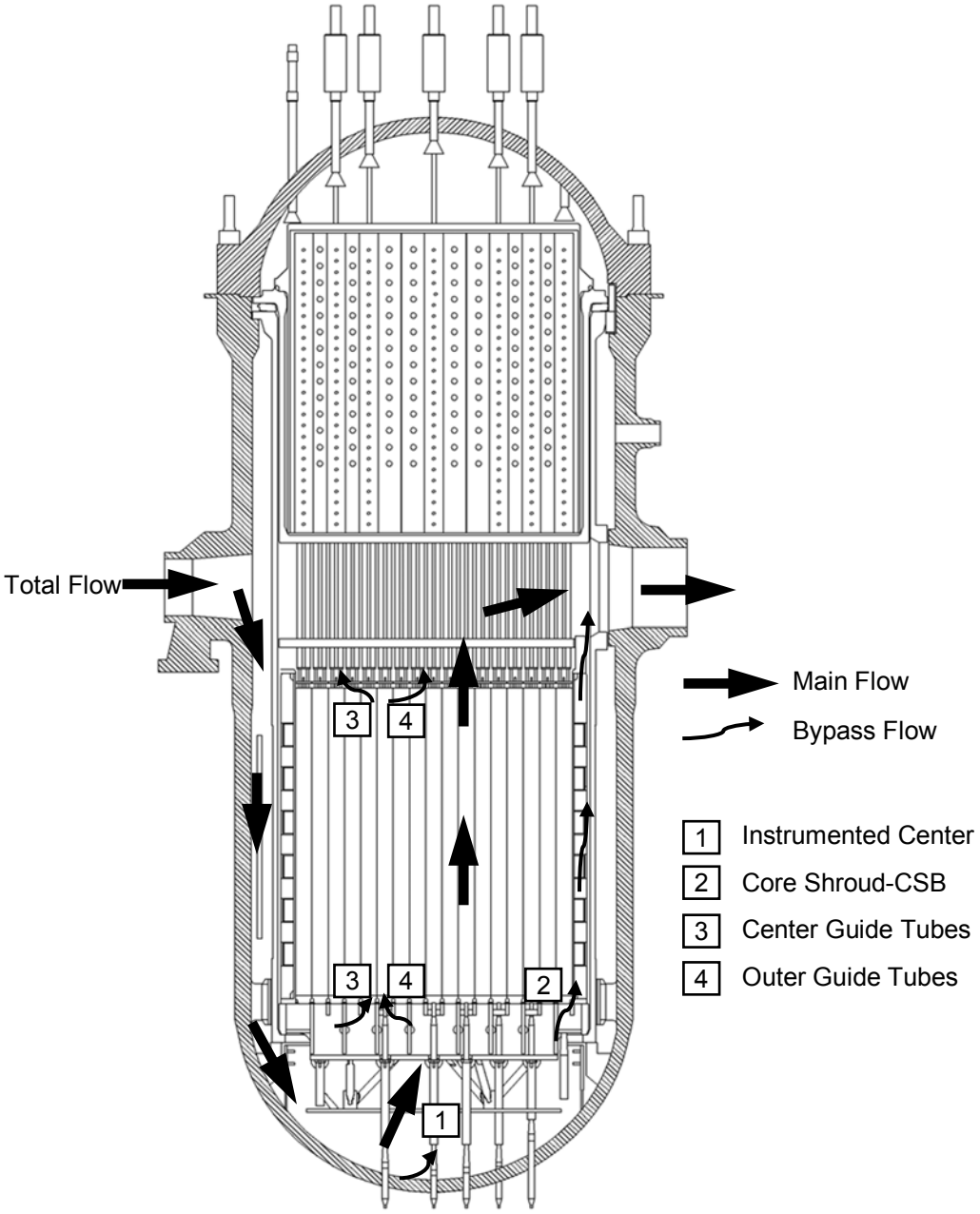

Figure 2.1-6 Flow Paths in the RV

2.2 APR1400 RVI Materials

Materials of the APR1400 RVI satisfy the requirements of ASME Section III NG-2000 (Reference 6). The material used in the fabrication of the reactor internals and core support structures is primarily Type 304 stainless steel. Welded connections are used where feasible. Table 2.2-1 shows a list of the major components of the reactor internals and core support structures, together with their material specifications.

The weld rod filler materials used are stainless steel Type [ ]^{TS}.

Table 2.2-1 Typical Material List of APR1400 RVI TS

3 ANALYSES FOR IASCC AND VS

3.1 Overall Description

Figure 3.1 provides an activity flow chart generally describing the approach of IASCC and VS evaluation. At first, an RVI component list for the APR1400 is collected. The results are summarized in Section 2.2. Then initial screening is performed for the RVI components using their fluence values, which were calculated by the DORT computer program (Reference 7) during the RVI design. The screening criterion is the neutron fluence of 5×10^{19} n/cm^2 (> 1 MeV). This screening criterion is conservative because it is significantly small compared to the IASCC and VS threshold fluences (Reference 2). Based on the initial screening, evaluation scopes are determined for a functionality assessment that involves three kinds of computer code analyses: radiation transport analysis, computational fluid dynamics (CFD) analysis and structural analysis.

The model for each analysis is determined to include the RVI components that would be expected to be exposed to neutron fluence higher than 5×10^{19} n/cm^2. For the radiation transport analysis, the model includes the RVI components in the range of FAP to the bottom plate of lower support structure, including CS, the lower part of CSB, snubber lugs, support beams, etc. The scope of modelling is somewhat different for each of the analyses, in accordance with the purpose of each analysis and/or the results of the radiation transport analysis (Figure 3.1-2).

The range between the two dotted lines shown in Figure 3.1-2, is for the radiation transport analysis, which covers the RVI components that would be expected to be exposed to the neutron fluence higher than 5×10^{19} n/cm^2 that was previously mentioned. The range between the two dot-dot-dashed lines is for the CFD simulation, which interfaces with the structural analysis. However, to calculate more accurate temperature and pressure data, the model range is radially extended to include CSB, the UGS support plate, the RV shell and the parts of the hot leg and cold leg. The range between the dot-dashed and the dotted lines is for the structural analysis. A smaller range is selected because the result of radiation transport analysis shows that the neutron fluence of the top plate of the core shroud is below 5×10^{19} n/cm^2.

The radiation transport analysis in Section 3.2 provides information on neutron and gamma fluxes in the APR1400 RVI. Neutron and gamma fluxes are calculated both for three different boron concentrations during equilibrium fuel cycles, which represent the beginning, middle, and end of the cycle (BOC, MOC and EOC) and for conservative fuel cycles considering a conservative radial pin power distribution and axial power shape irrespective of BOC, MOC or EOC. Additionally, a low leakage core is utilized in this analysis. Neutron flux results have been related to the displacements per atom (dpa) occurring as a result of collision of the neutrons in the CS, CSB and LSS regions. Using neutron and gamma flux data, gamma heating is also evaluated in units of W/cm^3 for the RVI. The results of the radiation transport analysis are used as inputs to the CFD analysis in Section 3.3 and the structural analysis in Section 3.4.

The CFD analysis in Section 3.3 provides temperature and pressure distributions for the RVIs. This analysis computes the effects of heat transfer between the metal components and the surrounding fluid and heat generation within the metal components caused by neutron and gamma irradiation. The results of this calculation are metal temperatures and pressures, which are used as boundary conditions by the ANSYS computer code (Reference 8). These conditions correspond to a low leakage core, three states within the equilibrium fuel cycles (BOC, MOC, and EOC) and one state for the conservative fuel cycles. Each case was characterized by a different distribution of heat sources or neutron and gamma fluxes.

The structural analysis of CS, CSB, and LSS in Section 3.4 provides effective stress and strain fields during the 60-year plant lifetime. This analysis is a non-linear analysis because the mechanical properties of the material are continuously changing due to neutron irradiation as operation time passes. Using the neutron flux data from the irradiation analysis, and the temperatures and pressures from the CFD

analysis, transient analysis of the RVI is performed for 60 years of design life, which includes the initial 8 conservative fuel cycles (12 year operation) and remaining 32 equilibrium fuel cycles (48 year operation). However, it should be noted that if a 93 percent capacity factor of the APR1400 is assumed and considered, structural analysis is only required for 55.8 effective full power years of operation.

After the stress and strain fields, temperatures and the neutron fluence are calculated using the three types of computer code analyses, the susceptibilities to IASCC and VS of the RVI components are determined using the USERMAT module, which is developed by the EPRI (Reference 9).

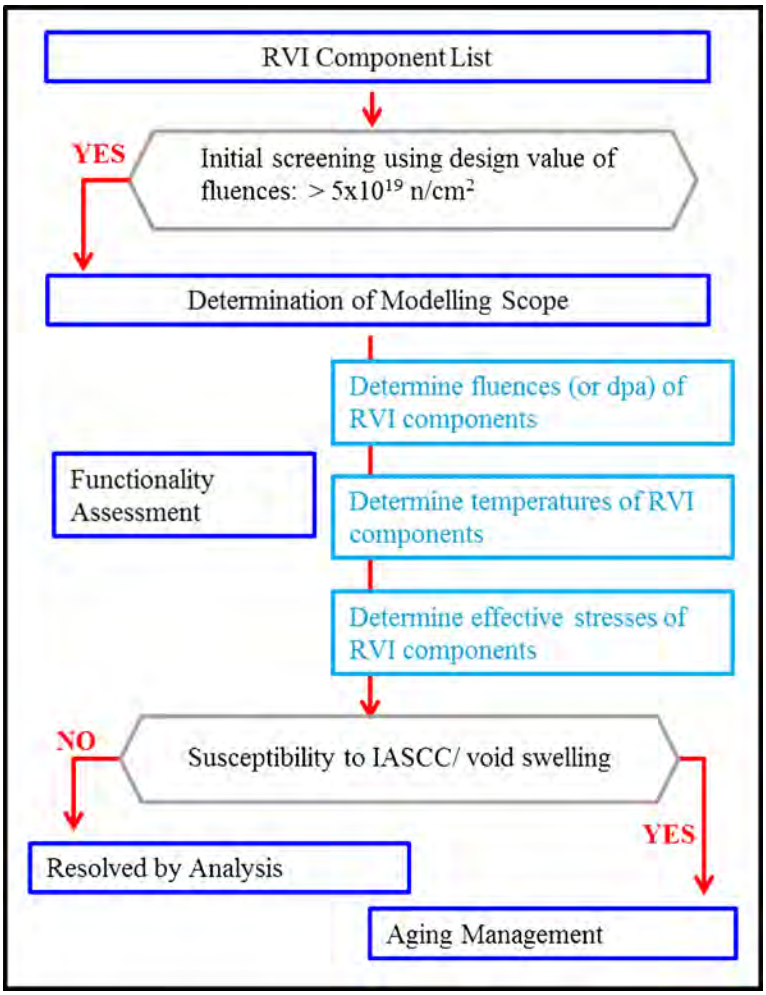

Figure 3.1-1 General Description of the IASCC and VS Evaluation Approach

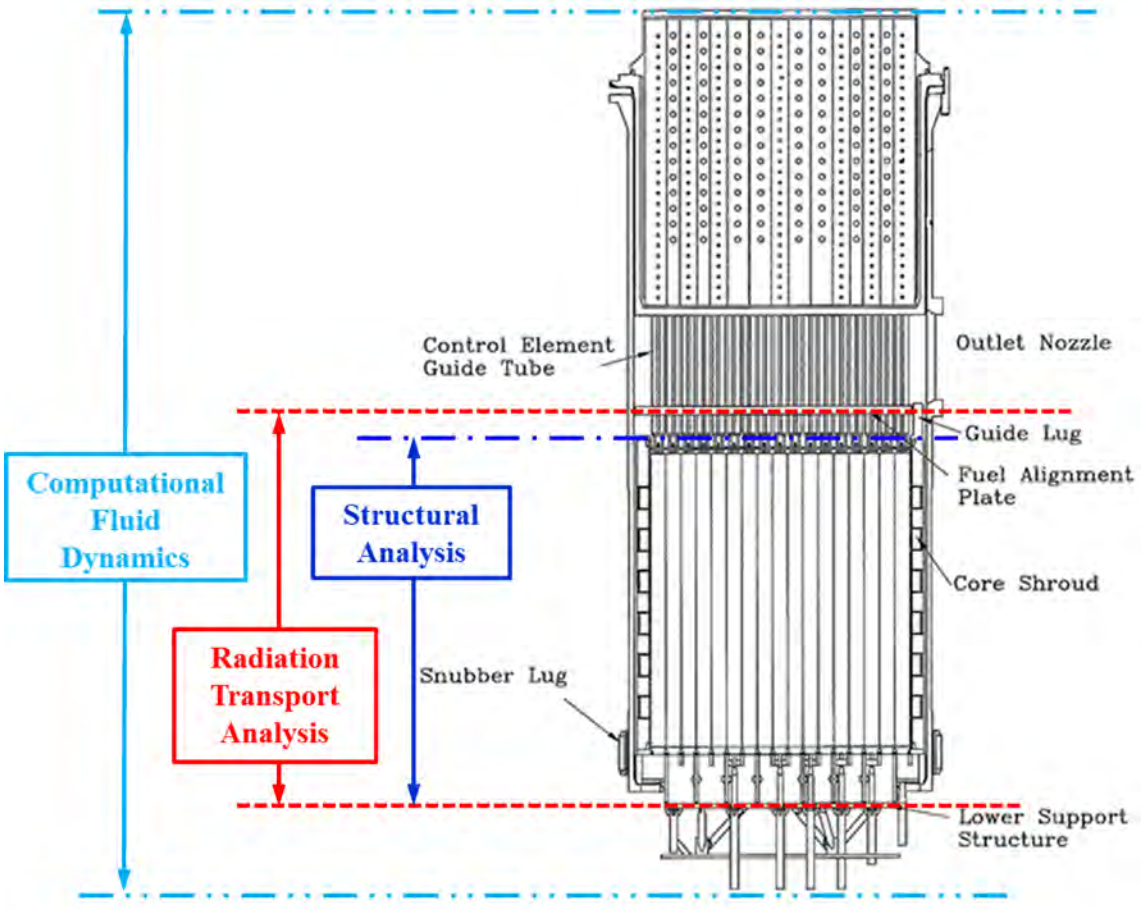

Figure 3.1-2 Model Scopes for Computer Code Analyses

3.2 Irradiation Transport Analysis

3.2.1 Analysis Computer Code

The MCNP code (Monte Carlo N-Particle Transport Code), version 5, build 1.60 (Reference 10) is used for calculating neutron flux (or dpa rate) and gamma flux (or heat generation source) in the APR1400 RVI. Even though irradiation transport analysis using two-dimensional DORT code has been performed for the APR1400 RVI, a reanalysis with three-dimensional MCNP code is conducted to obtain more accurate irradiation related information.

3.2.2 Calculation of Neutron and Gamma Flux

The neutron and gamma flux calculations for the APR1400 RVI are performed for a quarter (1/4) core model using the MCNP code and the point-wise ENDF cross section libraries developed by Brookhaven National Laboratory. Point-wise ENDF/B-VII and ENDF/B-VI cross section libraries (References 11 and 12) are used for neutron and gamma flux calculation, respectively. The quarter core model with mirror boundary condition is applied since the core has a symmetric structure.

Figure 3.2-1 shows XY-plane and XZ-plane cuts of the three-dimensional APR1400 RVI model. The calculation model includes fuel assemblies, FAP, CS, CSB, LSS, reactor vessel wall, primary shield, etc. The details of the model are shown in Figures 3.2-2 to 3.2-6.

MCNP calculations are performed for conservative fuel cycles and equilibrium fuel cycles. For the equilibrium fuel cycles, the different boron concentration stages of a fuel cycle, which represent BOC, MOC and EOC are considered for the calculation. Therefore, different axial power distributions are applied to the conservative fuel cycles and each of BOC, MOC and EOC of the equilibrium fuel cycles. The power distributions are shown in Figure 3.2-7. However, one radial power distribution is applied to the equilibrium fuel cycles without dividing into BOC, MOC and EOC in one fuel cycle.

Since the neutron and gamma fluxes depend mainly on the radial power distributions from the peripheral fuel assemblies, each pin power of the fuel rods in two rows of the outer peripheral fuel assemblies is considered for the equilibrium fuel cycles (see Table 3.2-1), but for the conservative fuel cycles, which are initial eight (8) fuel cycles, each pin power of the fuel rods in one row of the outer peripheral fuel assemblies is considered (see Table 3.2-2). The average value of the pin power of each fuel assembly is used for the corresponding assembly of the remaining assemblies.

A low leakage core is assumed in other to represent the APR1400 fuel loading pattern.

3.2.3 Calculation Results

The calculated neutron flux (dpa/sec) distributions in the APR1400 RVI components for the conservative fuel cycles and each of BOC, MOC and EOC of the equilibrium fuel cycles are shown in Figures 3.2-8 to 3.2-19; and the distributions of the calculated heat generation source are depicted in Figures 3.2-20 to 3.2-31. For the clear view, the neutron flux and heat generation data are depicted on the ANSYS RVI models described in Para. 3.4, and the rings do not appear in the figures of the CS. It should be noted, however, that the neutron flux and heat generation source values depicted in Figures 3.2-8 to 3.2-19 have been conservatively modified by adding [ ]^{TS} to the originally calculated values.

Table 3.2-1 Radial Assembly-averaged Power Distribution of the Equilibrium Fuel Cycle

TS

Table 3.2-2 Radial Assembly-averaged Power Distribution of Conservative Fuel Cycle

TS

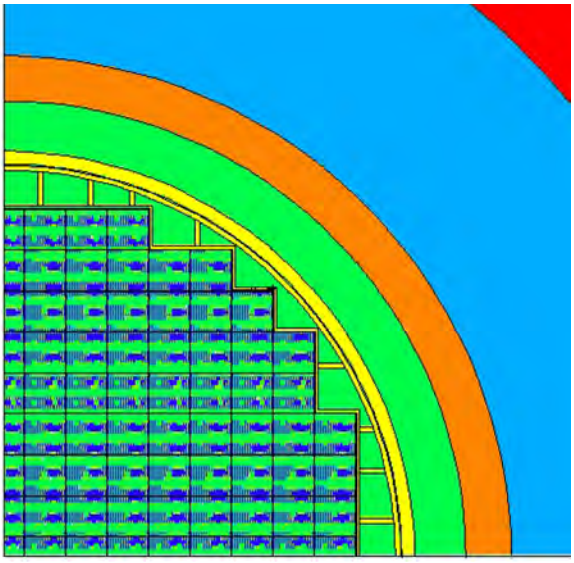

(a) XY-plane

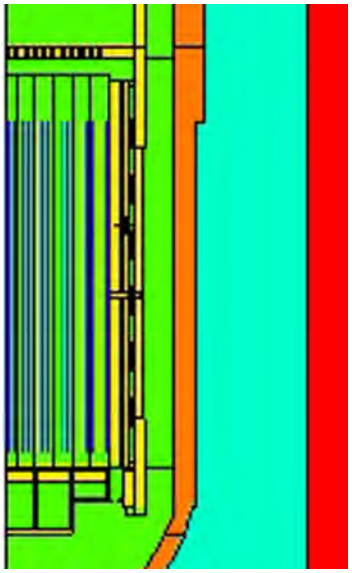

(b) XZ-plane

Figure 3.2-1 XY and XZ Plane Cuts of the APR1400 RVI Model

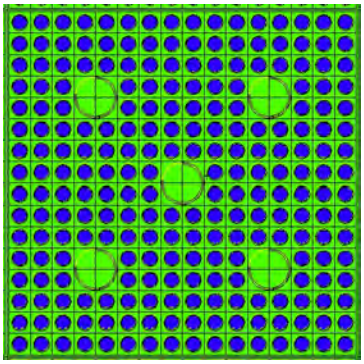

(a) XY-plane

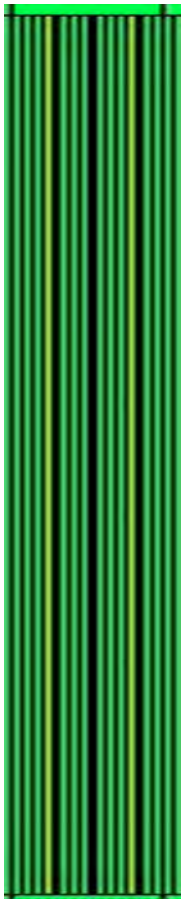

(b) XZ-plane

Figure 3.2-2 XY and XZ Plane Cuts of the Fuel Assembly Model

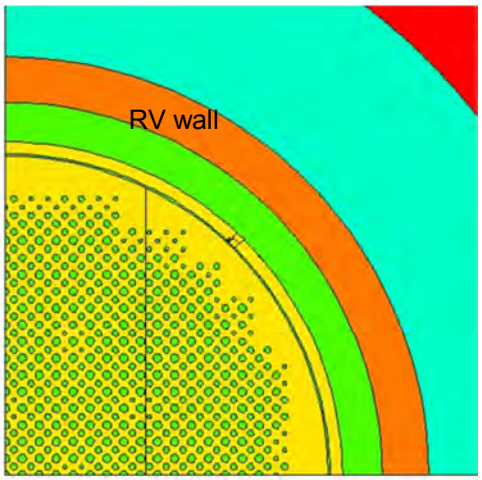

Figure 3.2-3 Model for FAP

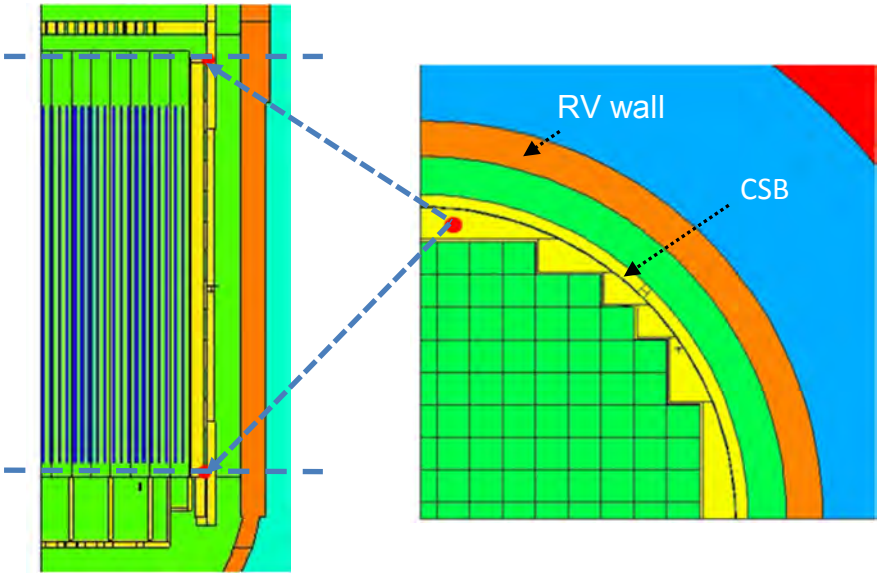

Figure 3.2-4 Models for Top and Bottom Plates

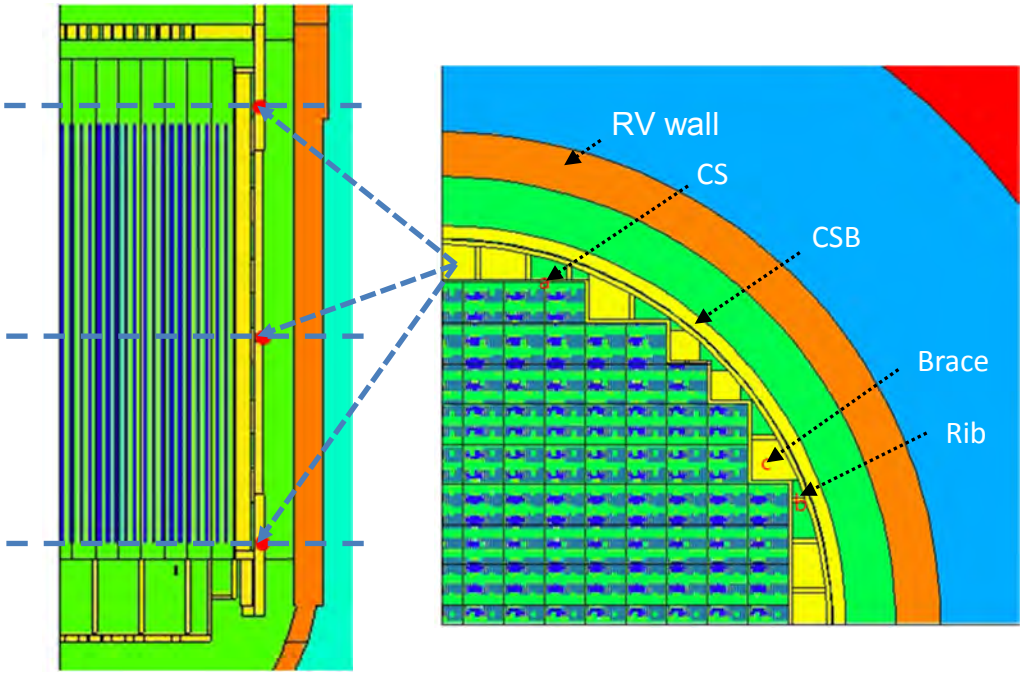

Figure 3.2-5 Models for CS, CSB, Rib and Brace

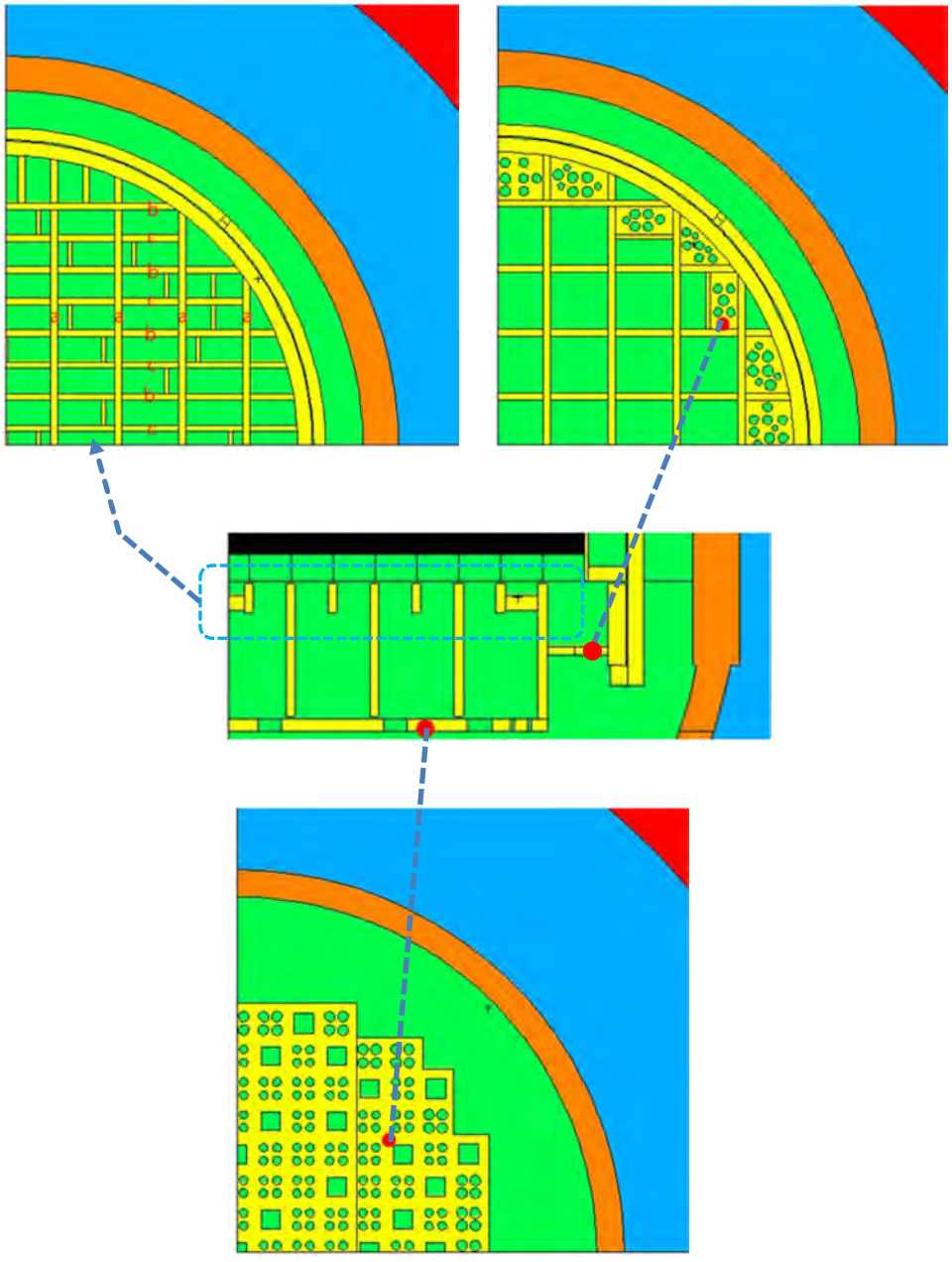

Figure 3.2-6 Model for LSS

Figure 3.2-7 Axial Power Distribution Profile

TS

Figure 3.2-8 Neutron Flux (dpa/sec) Distribution in CS (Conservative Fuel Cycles)

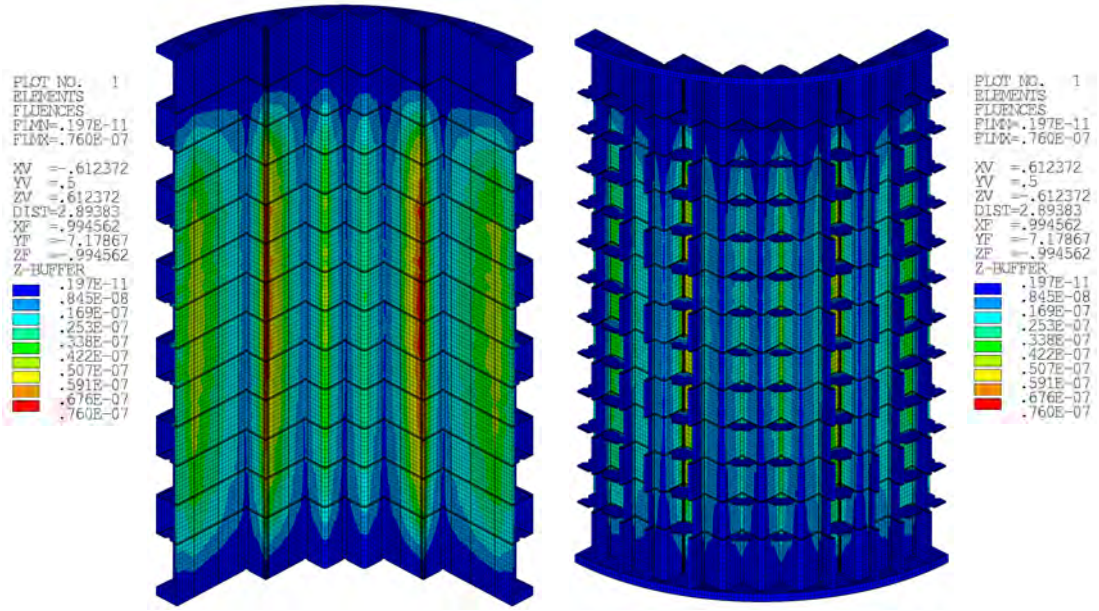

Figure 3.2-9 Neutron Flux (dpa/sec) Distribution in CS (BOC)

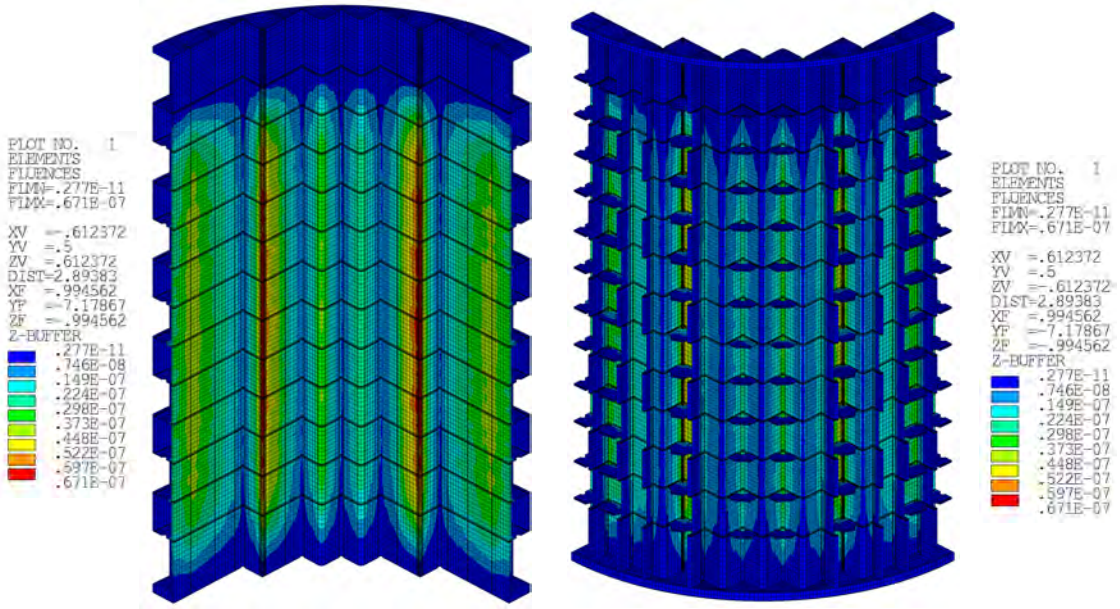

Figure 3.2-10 Neutron Flux (dpa/sec) Distribution in CS (MOC)

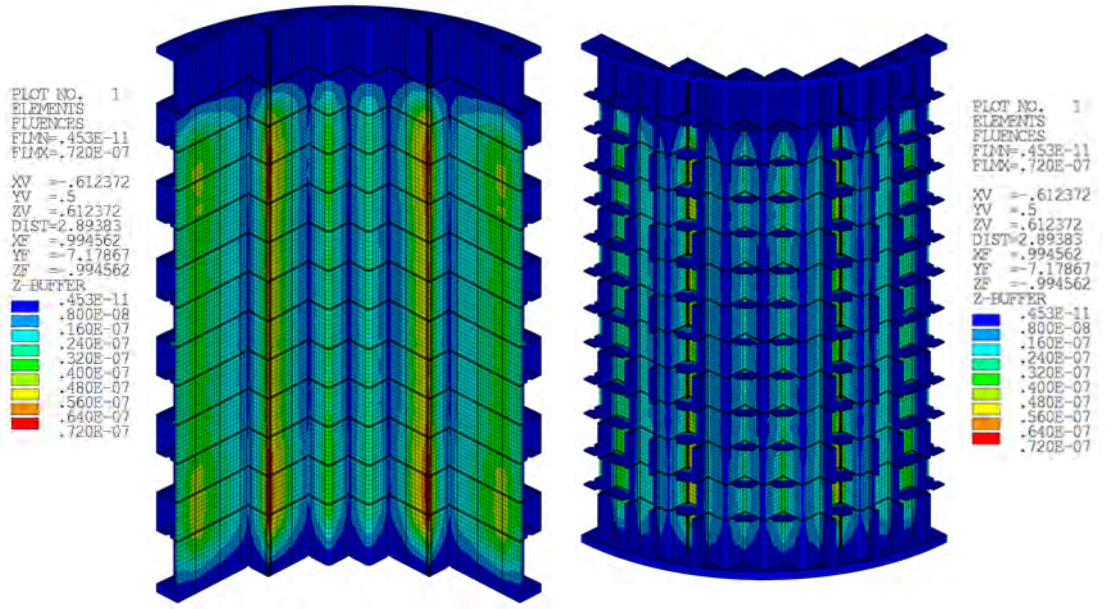

Figure 3.2-11 Neutron Flux (dpa/sec) Distribution in CS (EOC)

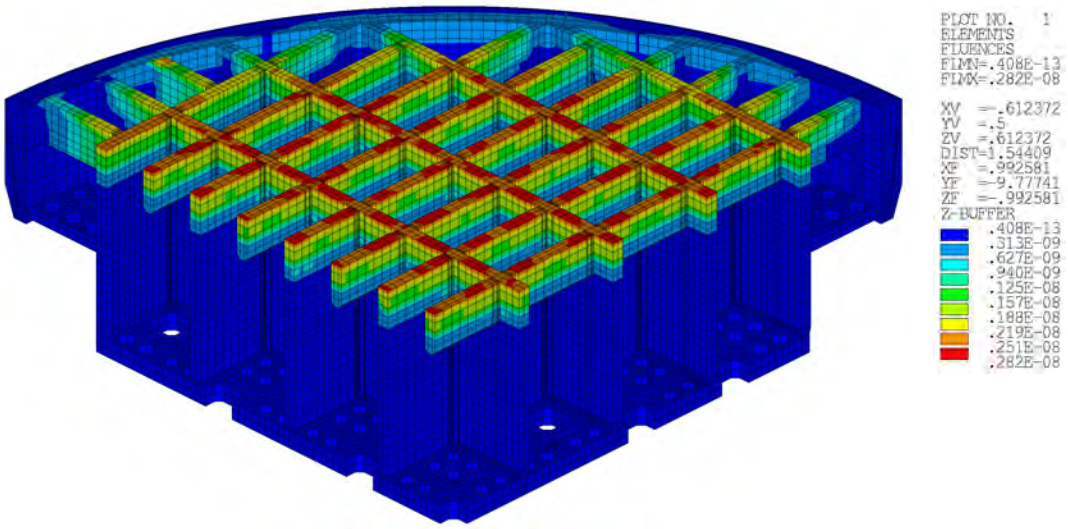

Figure 3.2-12 Neutron Flux (dpa/sec) Distribution in LSS (Conservative Fuel Cycles)

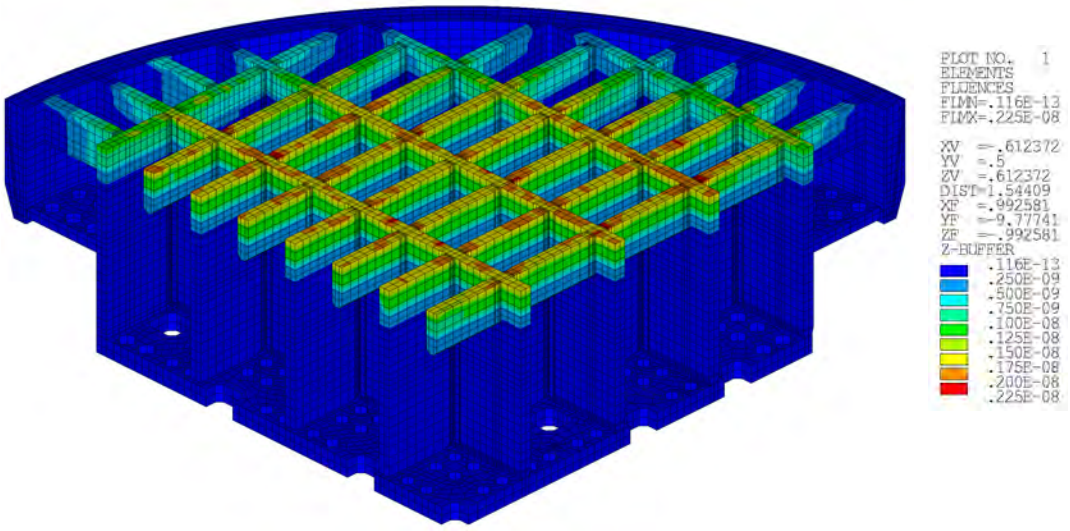

Figure 3.2-13 Neutron Flux (dpa/sec) Distribution in LSS (BOC)

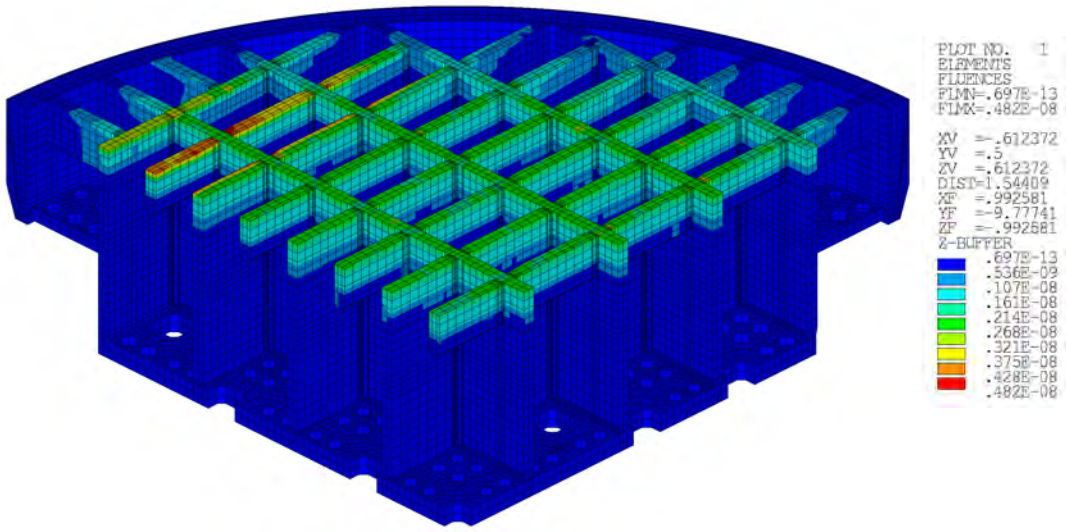

Figure 3.2-14 Neutron Flux (dpa/sec) Distribution in LSS (MOC)

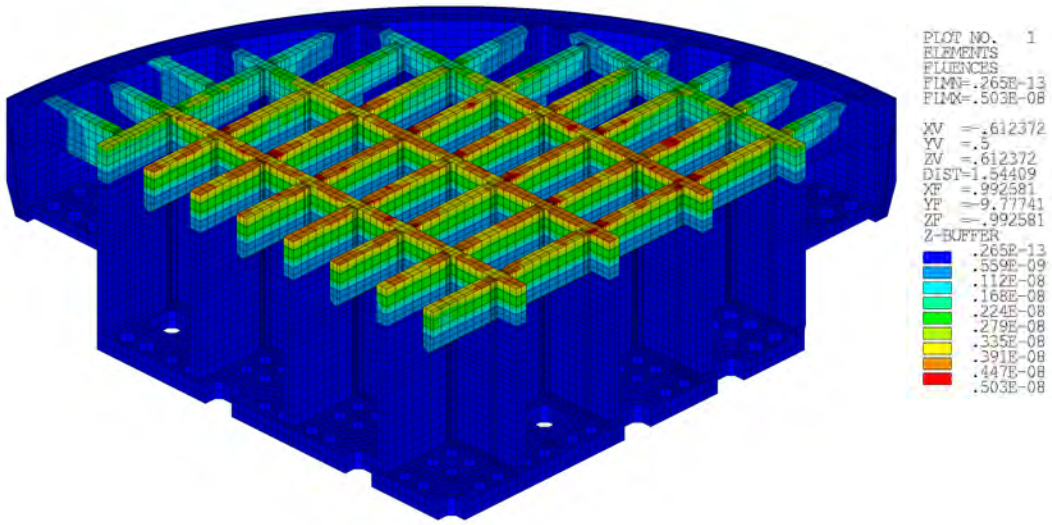

Figure 3.2-15 Neutron Flux (dpa/sec) Distribution in LSS (EOC)

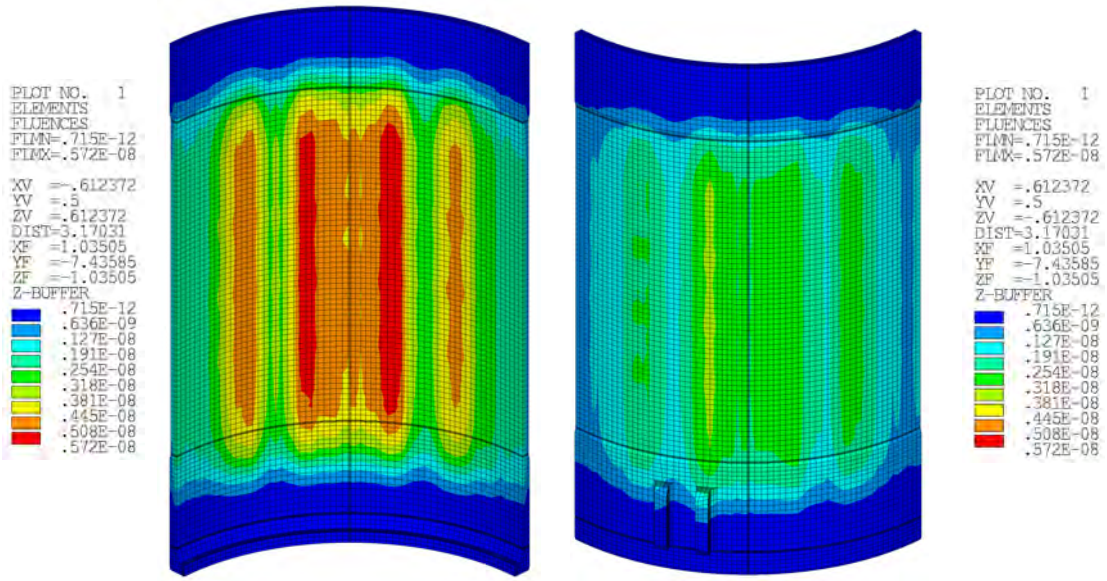

Figure 3.2-16 Neutron Flux (dpa/sec) Distribution in CSB (Conservative Fuel Cycles)

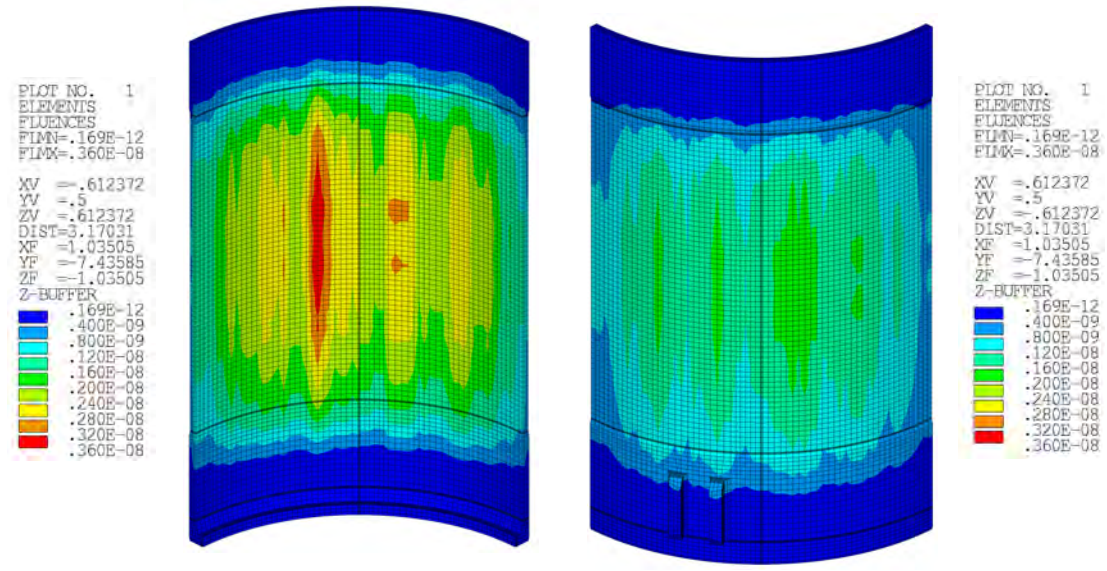

Figure 3.2-17 Neutron Flux (dpa/sec) Distribution in CSB (BOC)

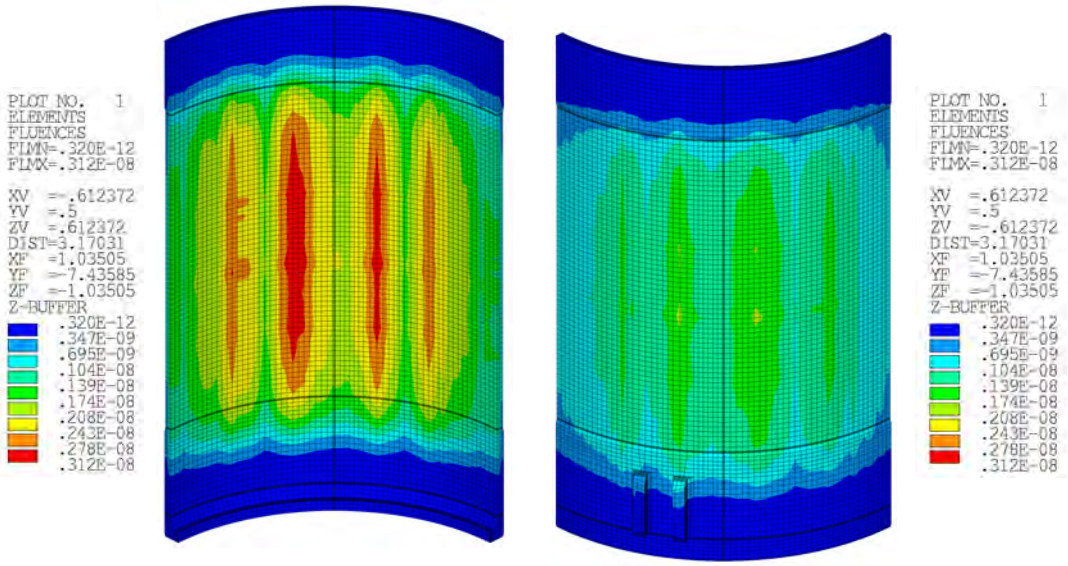

Figure 3.2-18 Neutron Flux (dpa/sec) Distribution in CSB (MOC)

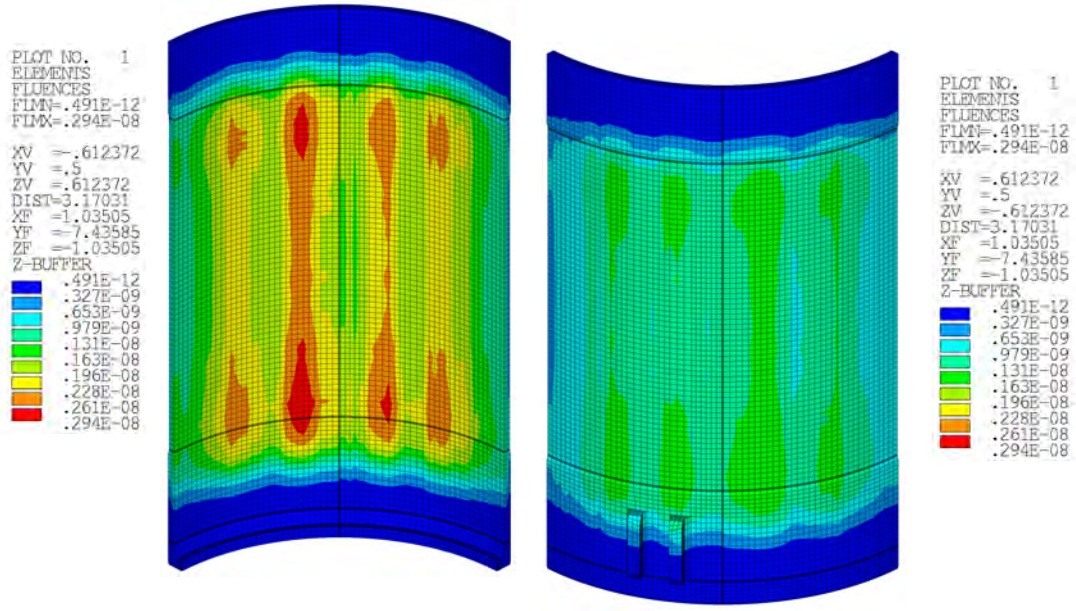

Figure 3.2-19 Neutron Flux (dpa/sec) Distribution in CSB (EOC)

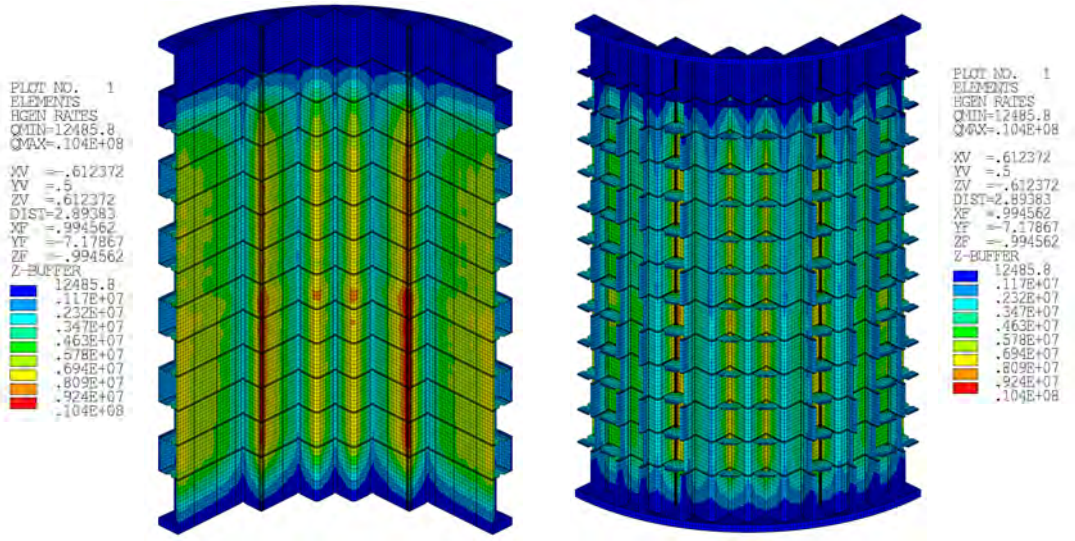

Figure 3.2-20 Heat Generation Source Distribution in CS (Conservative Fuel Cycles)

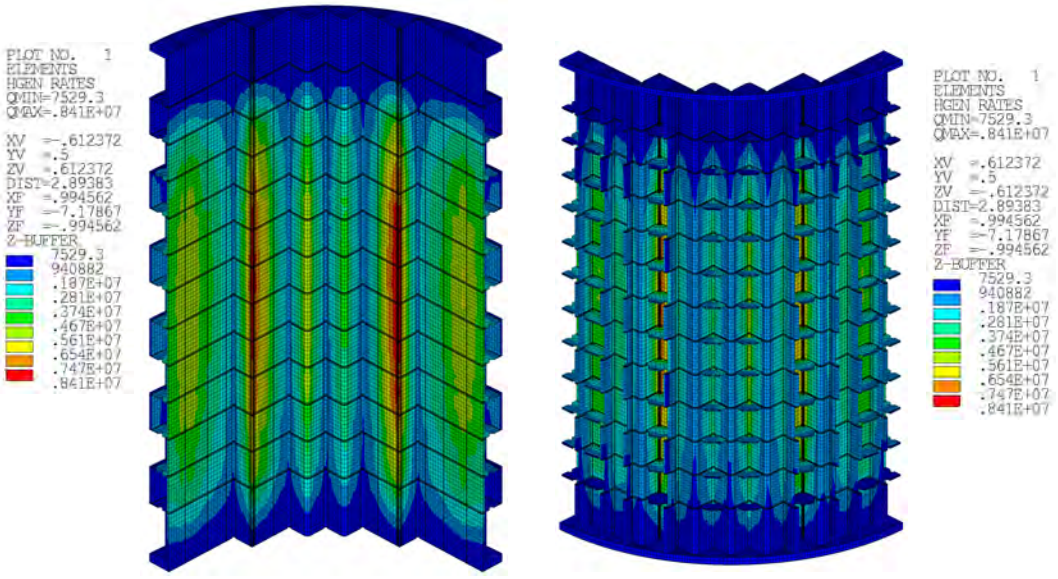

Figure 3.2-21 Heat Generation Source Distribution in CS (BOC)

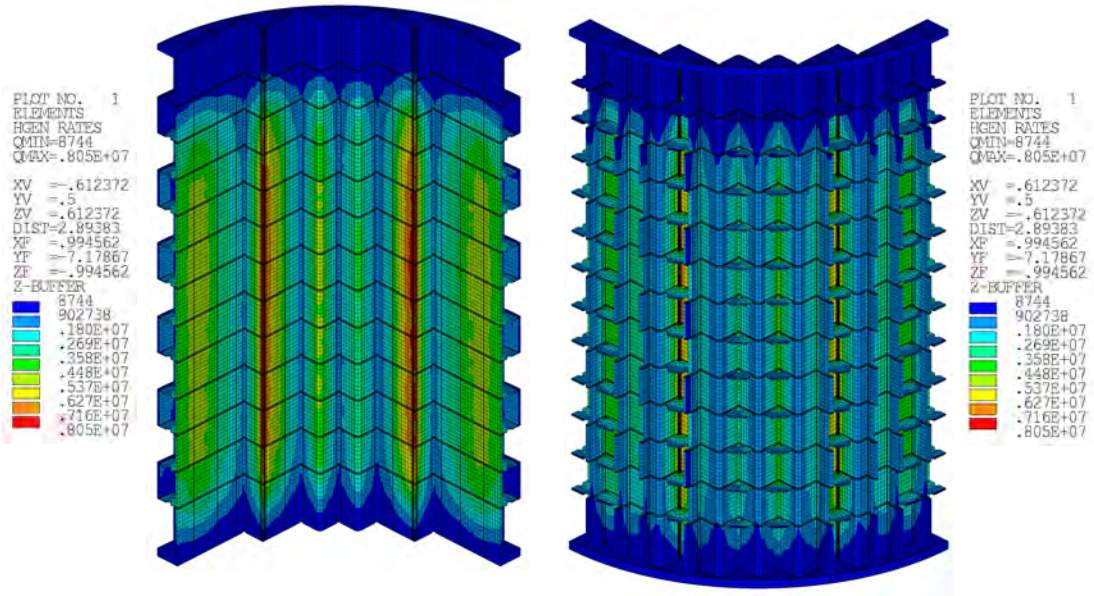

Figure 3.2-22 Heat Generation Source Distribution in CS (MOC)

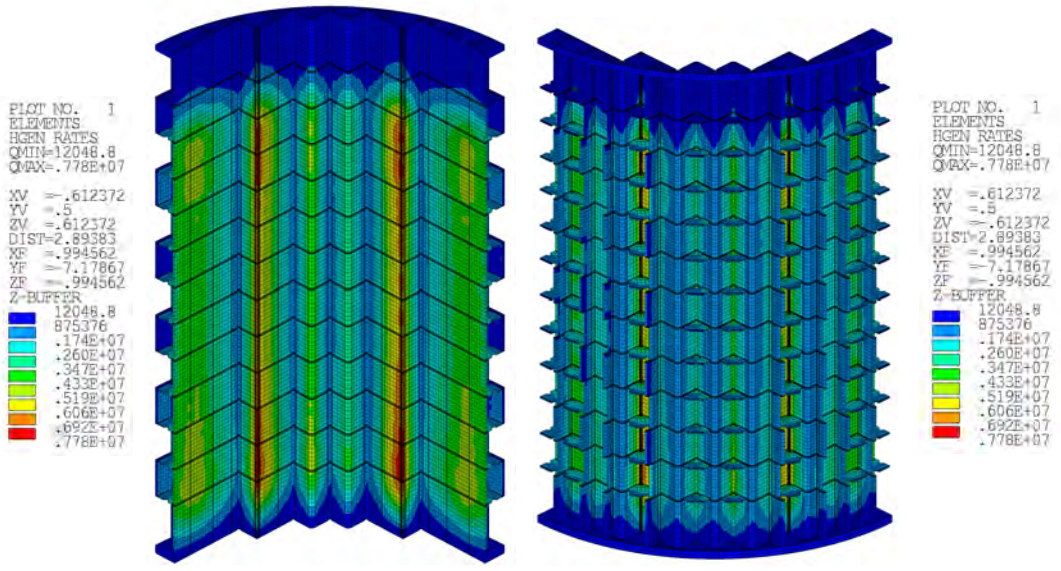

Figure 3.2-23 Heat Generation Source Distribution in CS (EOC)

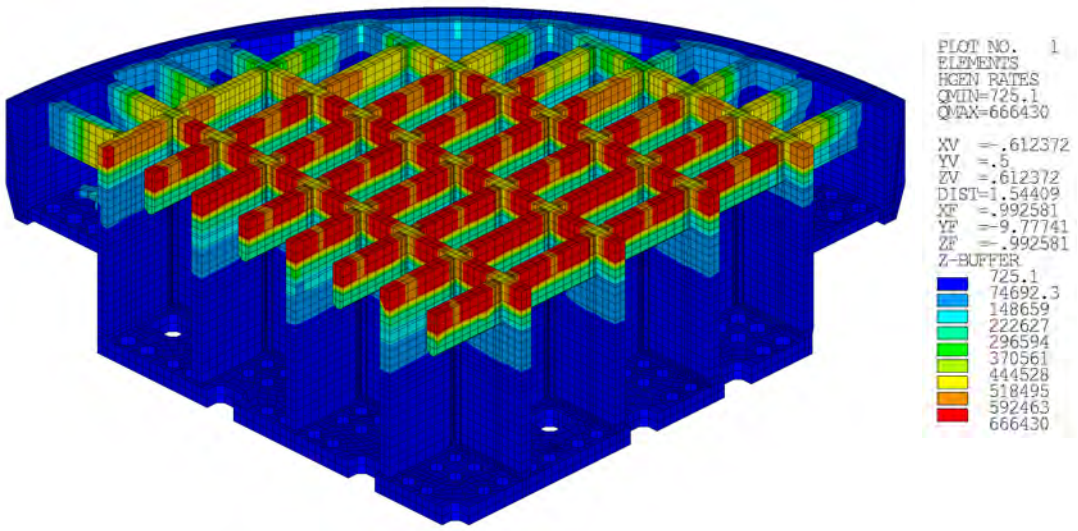

Figure 3.2-24 Heat Generation Source Distribution in LSS (Conservative Fuel Cycles)

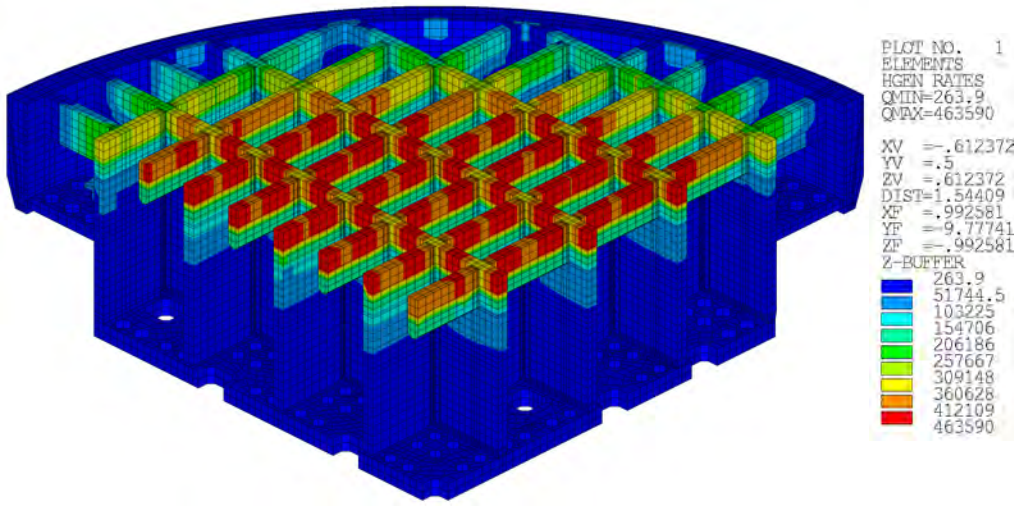

Figure 3.2-25 Heat Generation Source Distribution in LSS (BOC)

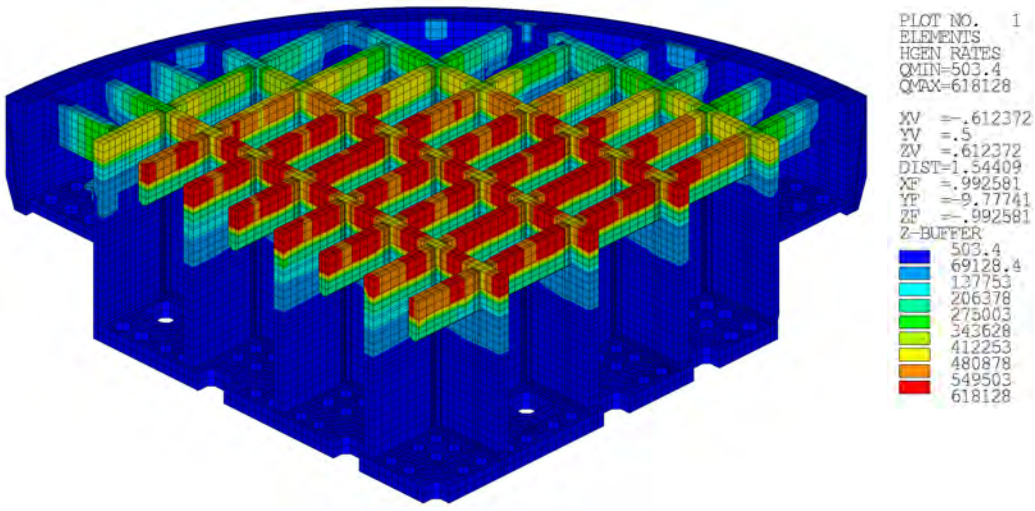

Figure 3.2-26 Heat Generation Source Distribution in LSS (MOC)

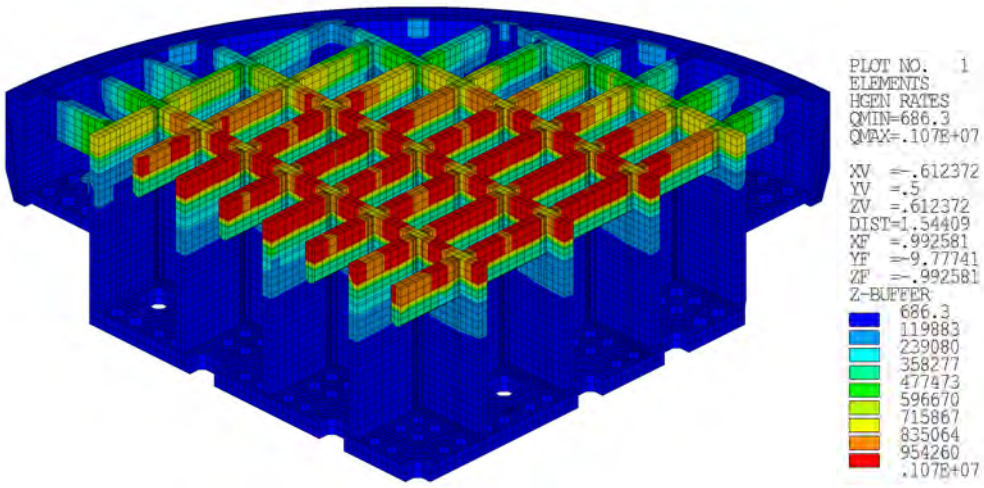

Figure 3.2-27 Heat Generation Source Distribution in LSS (EOC)

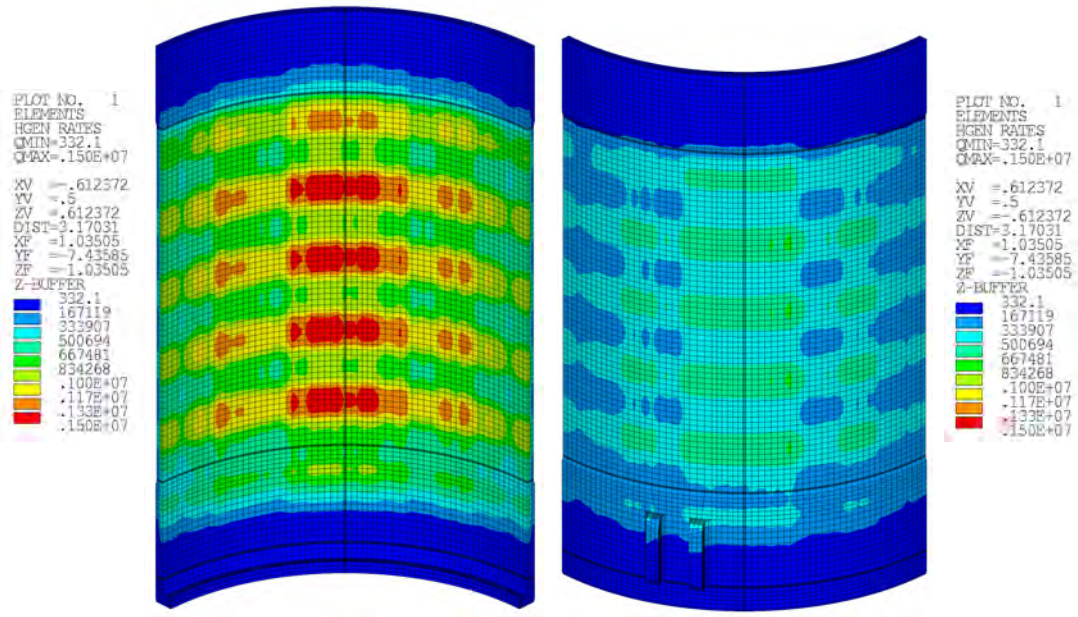

Figure 3.2-28 Heat Generation Source Distribution in CSB (Conservative Fuel Cycles)

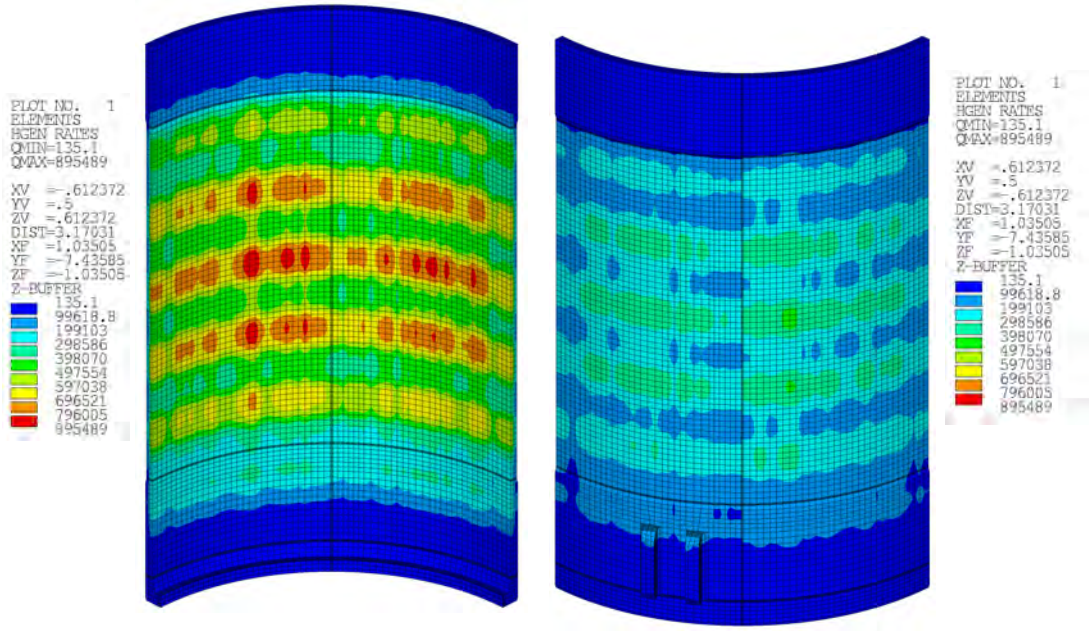

Figure 3.2-29 Heat Generation Source Distribution in CSB (BOC)

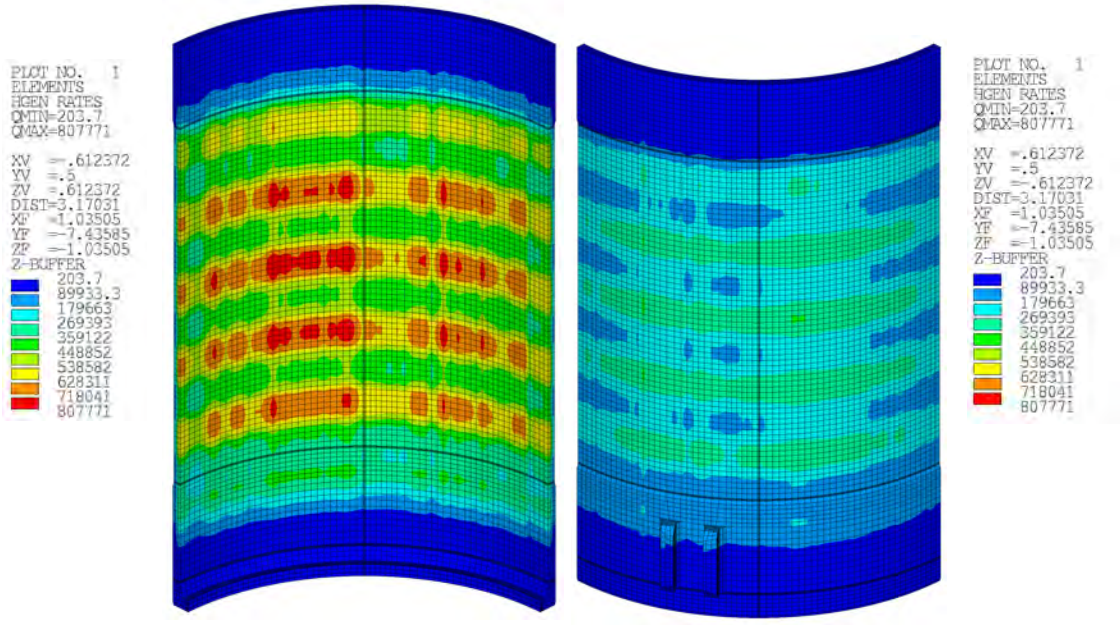

Figure 3.2-30 Heat Generation Source Distribution in CSB (MOC)

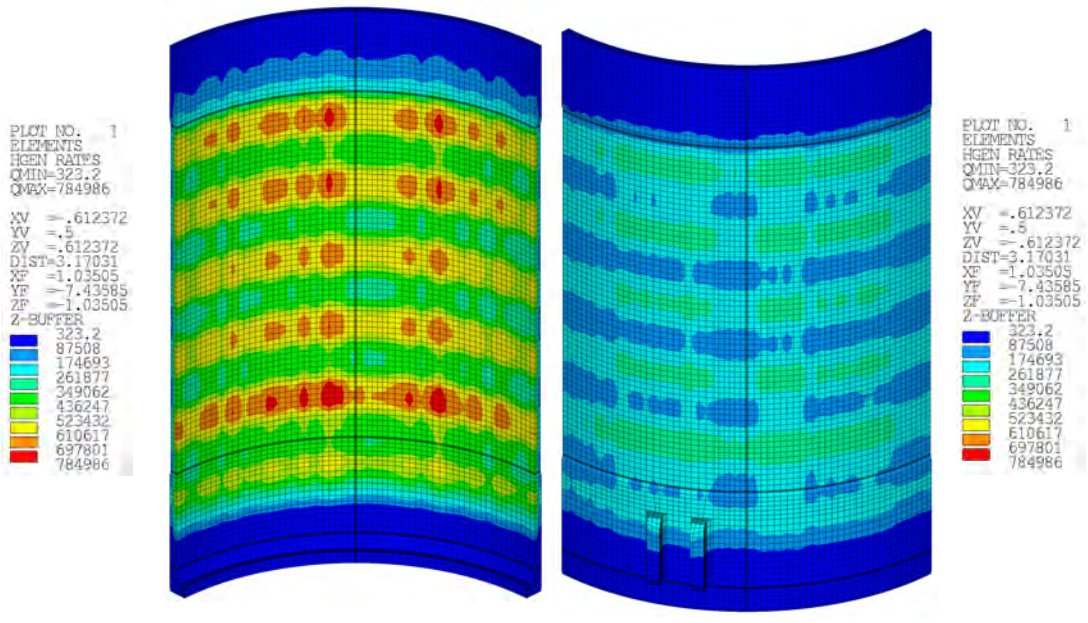

Figure 3.2-31 Heat Generation Source Distribution in CSB (EOC)

3.3 CFD Analysis

3.3.1 Analysis Computer Code

Computational Fluid Dynamics (CFD) code, STAR-CCM+ version 8 (Reference 13) is used to determine the temperature and pressure distributions in the RVI components by considering two things: the effects of heat transfer between the RVI components and the surrounding RCS coolant; and heat sources within RVI components caused by neutron and gamma irradiation.

3.3.2 Reactor Assembly Analysis

In the APR1400 reactor, there is a general difficulty in the application of test data and thermal experience when flow paths of various forms are combined. As a measure of the technical verification of the thermal flow characteristics in the experiment, it is difficult to obtain data except for actual measurement positions, to get derivations and correlations between measurement points and to find flow characteristics. CFD analysis techniques are applied in this study in order to get the necessary data in all regions inside the APR1400 reactor assembly and to quantitatively and systematically understand the heat flow phenomena. Numerical analysis for a nuclear reactor is performed in order to predict the thermal behavior and the flow of coolant and to analyze the distributions of the flow at the measurement positions and to determine the validity of the pressure drop.

For the CFD analysis model, Figures 3.3-1 and 3.3-2 show the main parts of the reactor assembly analysis model. The main shape is divided into Core shroud assembly, LSS + ICI guide assembly and LSS plate; in the upper guide structure, the major parts are the ICI, CS, Core, UGS, CSB, LSS and Rings.

3.3.2.1 Simulation Conditions

Although there are various turbulence models such as one equation models, LES (Large Eddy Simulation), and RSM (Reynolds Stress Model). The k-ω SST model is applied in this study in order to bolster the efficiency and accuracy of the solution. The k-ω SST model, used at the stage of analysis, is known to be excellent in accuracy and efficiency relative to the turbulence models.

The results are analyzed by running a fluid analysis of normal operation. The most important boundary condition is to reflect heat generation at the fuel core. The flow area can be divided into upper and lower regions. The inflow coolant from the upper region is heated at the fuel core which releases heat of 995.75 MWt (because of a quarter model), and exits through the outlet.

The working fluid is water; the flow rate, operation pressure and thermal power are shown in Table 3.3-1. The flow rate at the inlet flow of the reactor has a fully developed profile with a temperature of [ ]^{TS} °C in the tube; and the outlet is discharged at a temperature of [ ]^{TS} °C under normal condition.

Even during the fuel core and coolant heat transfer, the reactor outside is thermally shielded and there is no heat escape. Therefore, adiabatic conditions are considered to be those of no heat loss through the wall. The symmetry plane on both sides of the quarter model shows the adoption of symmetry conditions.

Material properties such as density, viscosity, conductivity, and specific heat are shown as polynomial functions of temperature in the solid and fluid models (See Table 3.3-2). The initial conditions of the flow area of the reactor assembly should have the following pressure and temperature: operating pressure, [ ]^{TS} MPa; operating temperature, [ ]^{TS} °C.

Figure 3.3-3 illustrates the boundary conditions of the inlet and outlet. Inlet flow is applied at the flow rate condition of the pump discharge, which is divided into four equal parts of the [ ]TS kg/s in a quarter model. Prior to the heat flow analysis, emission analysis from the fuel core is an advanced line; the values of the heat sources of CS, CSB, LSS and UGS are applied to the input values of CFD.

3.3.2.2 Assumption Conditions

Actually, the shape of the fuel core is very complex. To create grid systems for a very complex core shape is a high-cost problem. Therefore, a method for modeling is required that will not affect the analysis results. As previously mentioned, a porous media model is applied in the actual analysis based on the results of a single item experiment.

Porous media modeling is an approach to modeling that can be used to simulate the behavior of a fluid passing through the inner space filled with solid particles; it is used to simulate the same effect of, even if it does not implement the same form of, solid particles. The porous media model can be defined by flow resistance; porosity and pressure drop of the fluid can also have different values depending on the anisotropic direction.

It is possible to model the core device of the reactor assembly as a porous media with these characteristics. The pressure drop of the working fluid can be applied equally well to predict water flow as it passes through the core. Caused by the shape of the core, flows are shown to have large values in the axial direction.

The value of the pressure drop across the porous media is calculated as a function of the Eugen's type of velocity of the fluid. In the STAR-CCM +, the coefficients (P_i: inertial resistance, P_v: viscous resistance), appearing in the following equation, can be defined by the values of the pressure drop and the velocity (P-Q Curve), which are obtained in a different analysis.

$$\Delta P / L = (P_v + P_i |v|)v$$

Where, v is velocity.

In this analysis, in order to derive the coefficients of the quadratic function of the pressure drop, the actual shape is calculated for the respective flow rates. Figure 3.3-4 shows the correlation rate and the pressure difference in the inlet and outlet of the core device for each analysis case. Table 3.3-3 shows the calculated values of P_i, and P_v.

The effective thermal conductivity of the porous region is defined as the ratio of the open area to the total volume of the porous medium. This value is mainly used to mix the thermal conductivity of the solid and fluid materials.

3.3.3 Calculation Results

The effects of flow distribution have been compared with the change of the heat source size of the core (BOC, MOC, EOC and Conservative fuel cycle). The flow distributions of the horizontal cross section from the inner center and of the fuel core tip are compared in order to provide more detailed analysis results. The results for the cross section in the same position are extracted, as shown in Figure 3.3-5. Figures 3.2-6 to 3.3-8 show the temperature distributions in the cross section of the reactor bottom. Temperature distributions are similar overall and differences between the minimum and maximum values are relatively small (BOC ([ ]TS °C), MOC ([ ]TS °C), EOC ([ ]TS °C)). For location S2, temperature distribution values appear to have a similar trend, but it can be confirmed that the high point

of temperature is displayed in the order of BOC, MOC and EOC (See Figures 3.3-9 to 3.3-11). Temperature distributions in the reactor top are shown in Figures 3.3-12 to 3.3-14. Because the flows of the fuel core and the internal inlet are separated by the outer wall, the temperature distributions at the top of the fuel core can be seen to be relatively high, while the temperature is low on the outer wall.

Figures 3.3-15 to 3.3-17 show temperature distributions in the upper part of the reactor fuel core are at a very high level of about 326°C; this level is substantially similar in all operating conditions. The temperature at the center of the fuel core is the highest; it is relatively low on the outer wall by the coolant flow path.

Figures 3.3-18 to 3.3-20 show that the temperature distributions in the CS are high in the upper region due to the heat of the fuel core but they are relatively low at the bottom due to inflow of coolant. The high temperature in the center of the reactor at EOC is slightly larger than BOC or MOC. Therefore, the heat source and the operating conditions contribute to the temperature of parts.

The temperature and pressure distribution in the CS, CSB, LSS and UGS are used as the input value for structural analysis and identified in Tables 3.3-4 to 3.3-7.

It should be noted that the applied inputs to the CFD analysis include an additional [ ]^{TS} margin used in order to obtain conservative evaluation results.

Table 3.3-1 Design Specifications of the Reactor Analysis **TS**

Table 3.3-2 Material Properties

TS

Table 3.3-3 Porous Media Resistance Tensor

TS

Table 3.3-4 BOC CFD Data Results

TS

Table 3.3-5 MOC CFD Data Results

TS

Table 3.3-6 EOC Data Results

TS

Table 3.3-7 Conservative CFD Data Results

TS

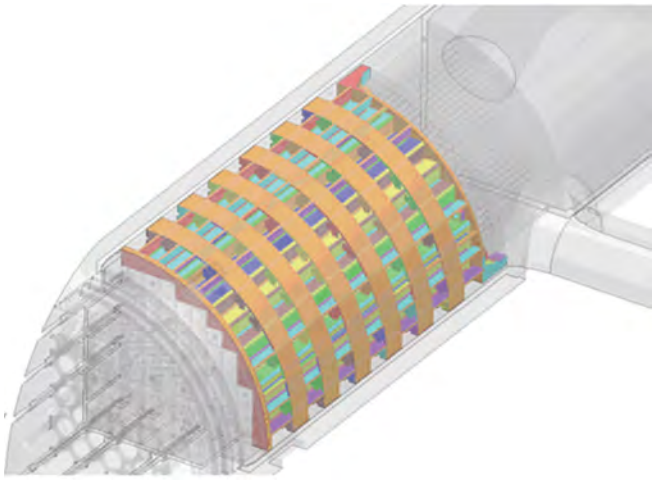

Figure 3.3-1 Core Shroud Assembly

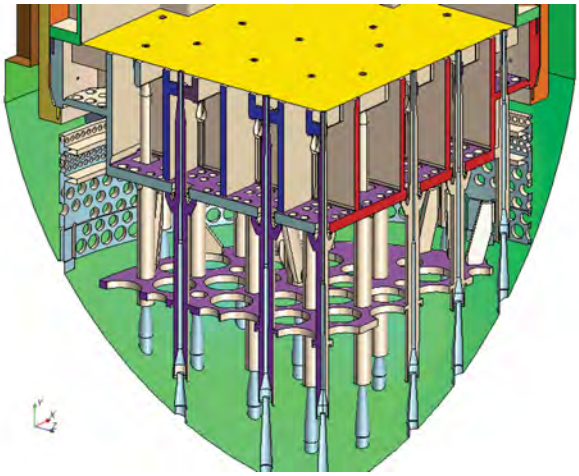

Figure 3.3-2 LSS+ICI Nozzle Assembly

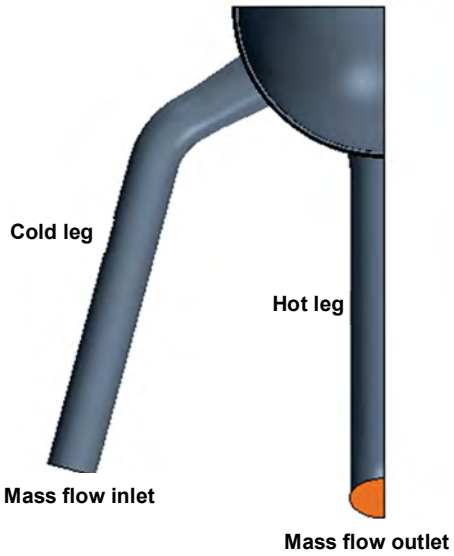

Figure 3.3-3 Boundary Conditions of the Reactor Assembly

TS

Figure 3.3-4 Boundary Conditions of the Reactor Assembly

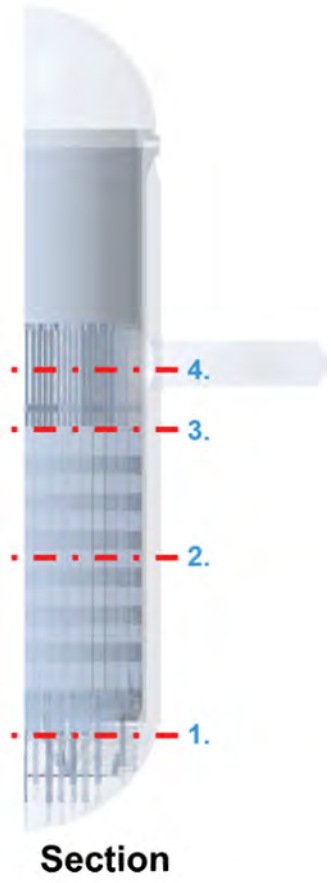

Figure 3.3-5 Position of the Section to Check the Flow in the Reactor

Figure 3.3-6 Temperature Distributions at the S1 Section (BOC)

Figure 3.3-7 Temperature Distributions at the S1 Section (MOC)

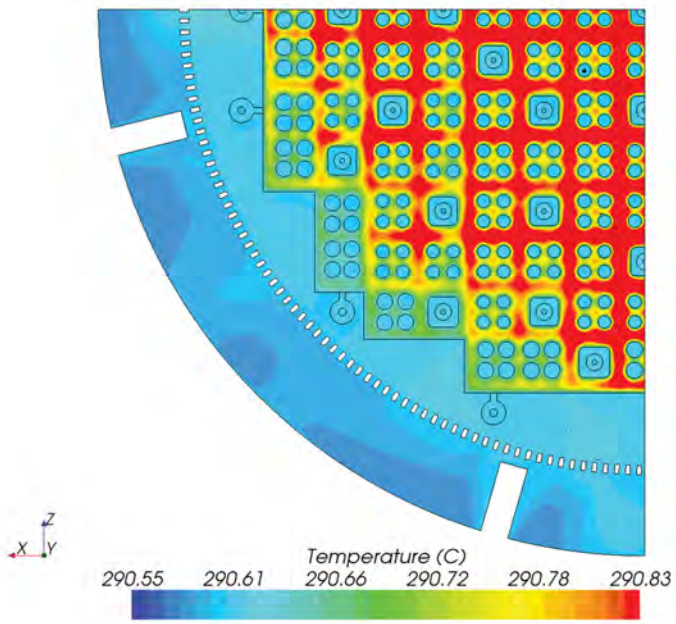

Figure 3.3-8 Temperature Distributions at the S1 Section (EOC)

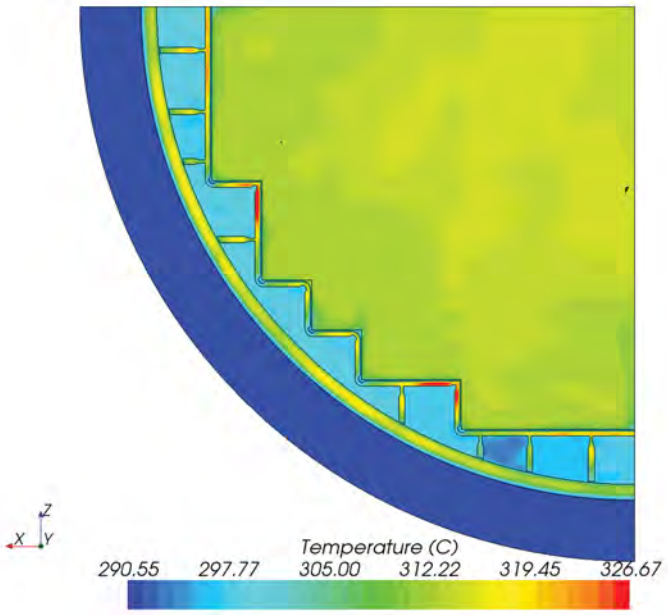

Figure 3.3-9 Temperature Distributions at the S2 Section (BOC)

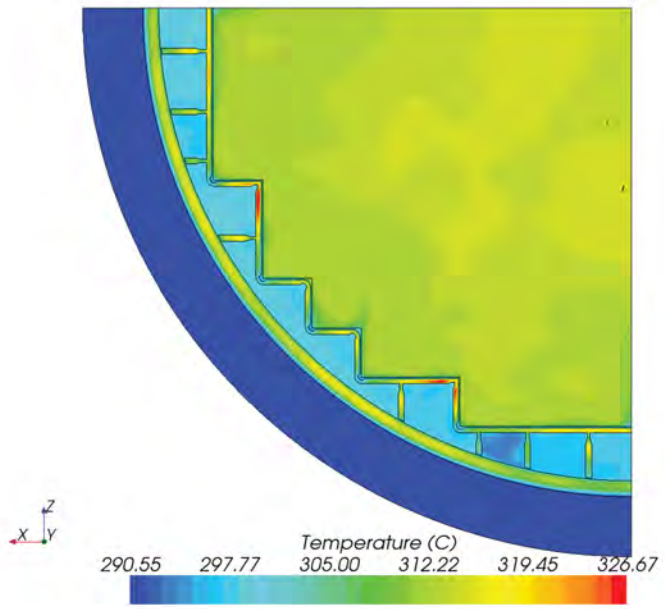

Figure 3.3-10 Temperature Distributions at the S2 Section (MOC)

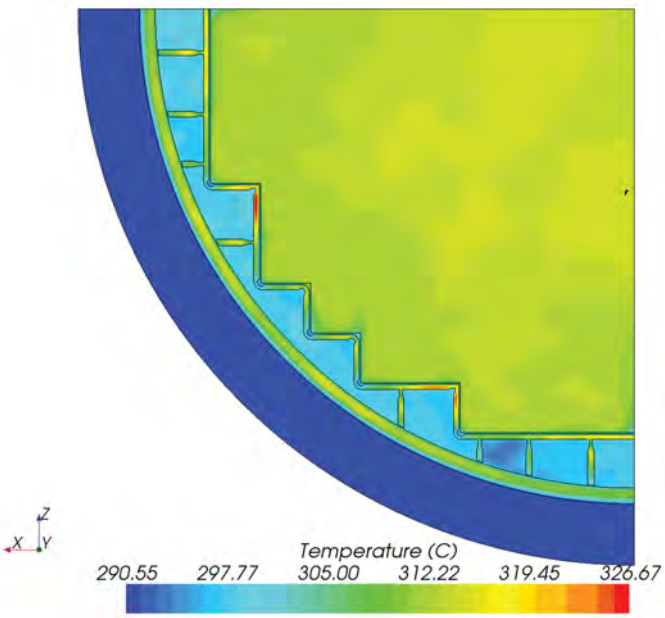

Figure 3.3-11 Temperature Distributions at the S2 Section (EOC)

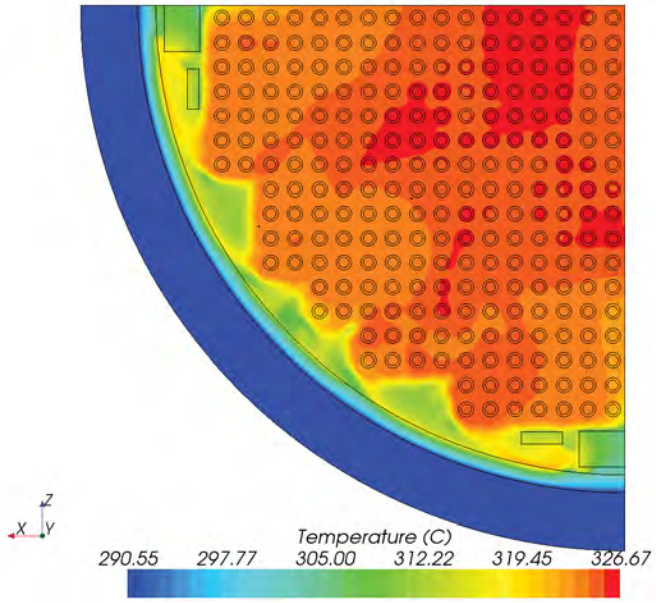

Figure 3.3-12 Temperature Distributions at the S3 Section (BOC)

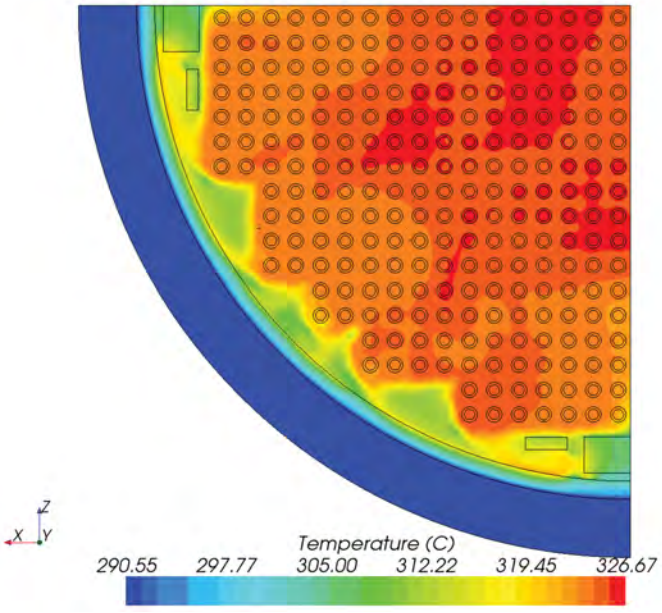

Figure 3.3-13 Temperature Distributions at the S3 Section (MOC)

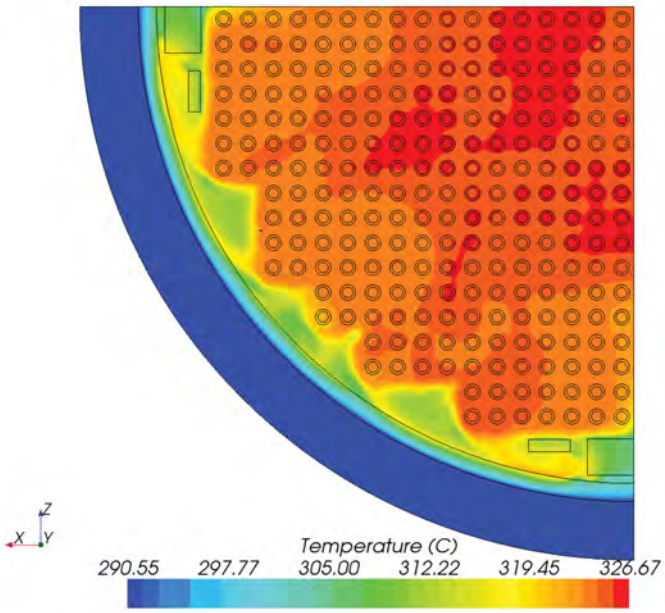

Figure 3.3-14 Temperature Distributions at the S3 Section (EOC)

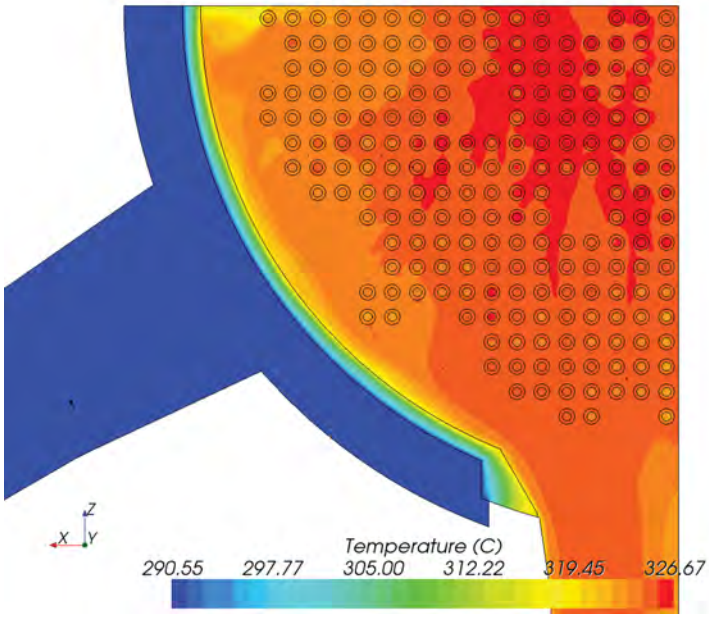

Figure 3.3-15 Temperature Distributions at the S4 Section (BOC)

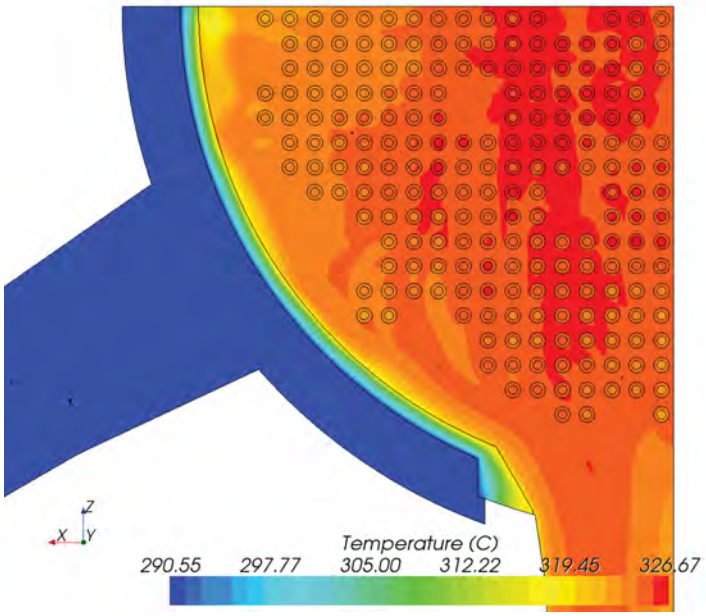

Figure 3.3-16 Temperature Distributions at the S4 Section (MOC)

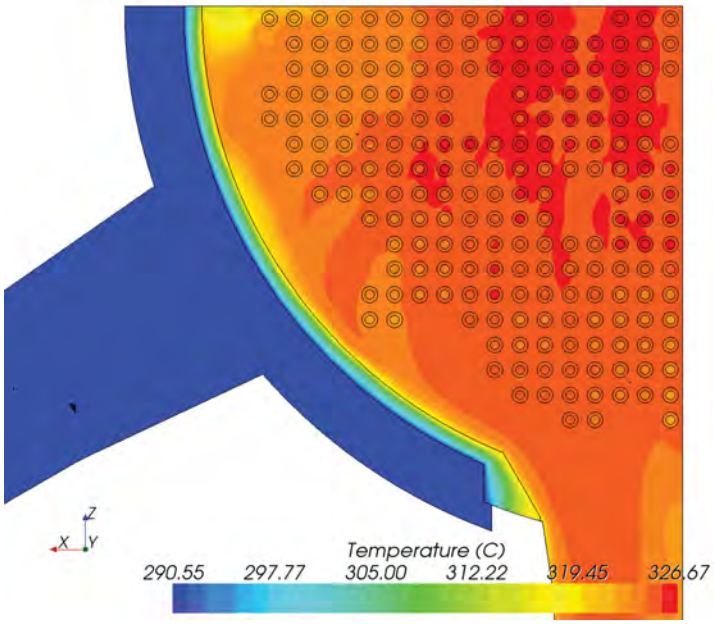

Figure 3.3-17 Temperature Distributions at the S4 Section (EOC)

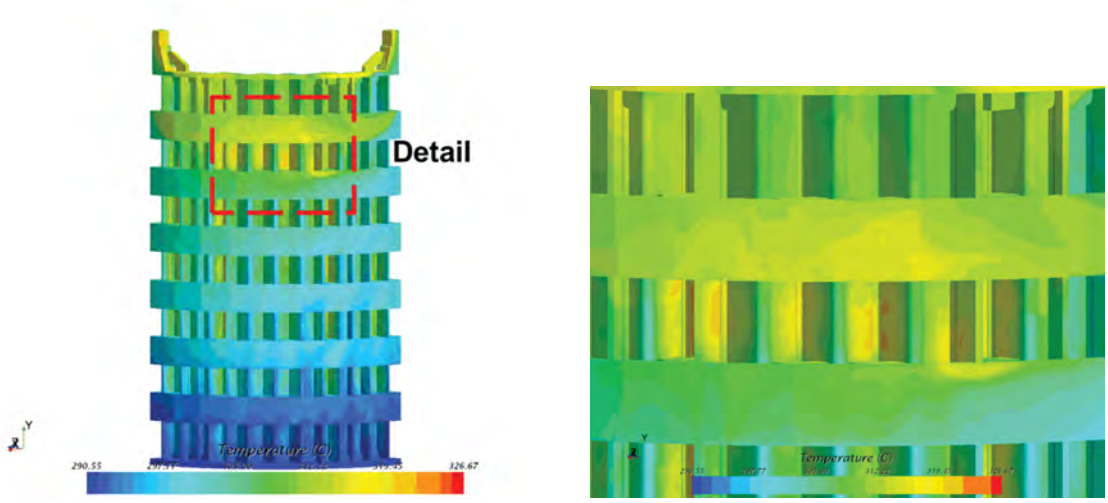

Figure 3.3-18 Temperature Distributions on the CS (BOC)

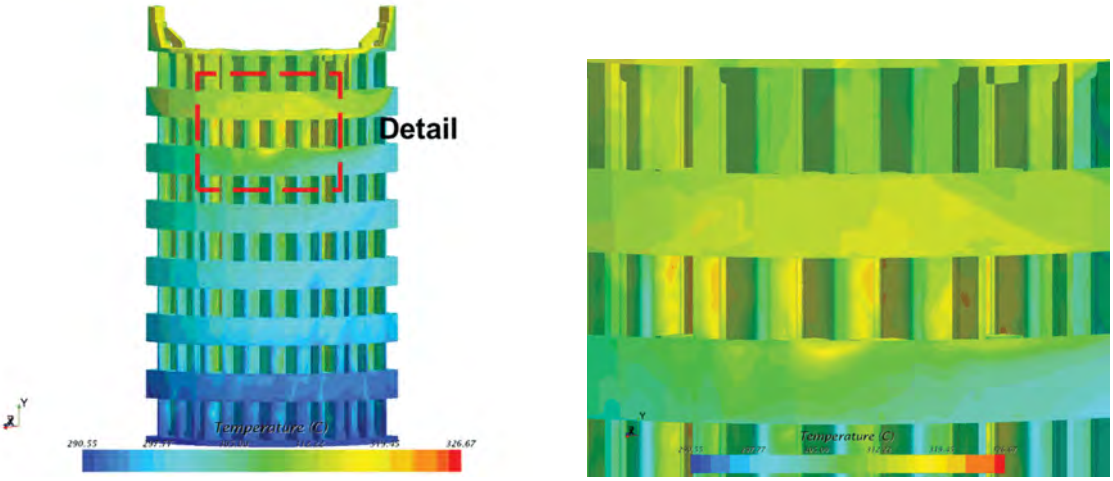

Figure 3.3-19 Temperature Distributions on the CS (MOC)

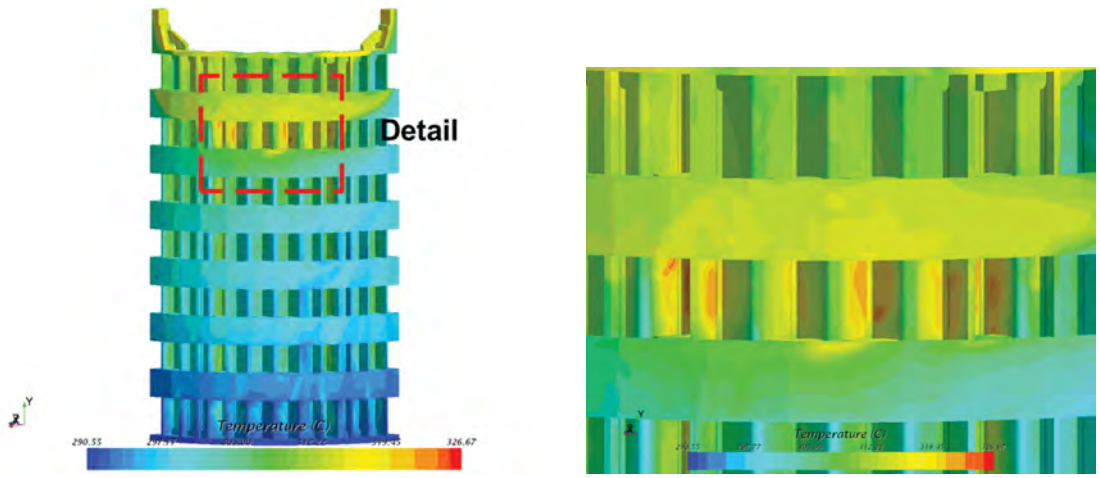

Figure 3.3-20 Temperature Distributions on the CS (EOC)

3.4 Structural Analysis

3.4.1 Analysis Computer Code

The general purpose finite element code ANSYS (Reference 8) is used to perform the structural evaluations of the APR1400 RVI components. Since the mechanical properties of the RVI materials change as a function of temperature and neutron fluence, the resulting stress and strain fields are calculated by the ANSYS code with a subroutine called “USERMAT”, which uses the constitutive equations for typical irradiated RVI materials that are depicted in MRP-135 (Reference 14). The Usermat.f subroutine, version 3.12 (Reference 9) is used to perform the material degradation calculations. The results are represented in terms of state variables (SVs). The IASCC susceptibility ratio (SV10) is used for the evaluation of IASCC, and effective irradiation growth strain (SV3) is used for the evaluation of VS.

3.4.2 Finite Element (FE) Models

Quarter (1/4) finite element models are developed for IASCC and VS evaluation of the APR1400 RVI, including CS, LSS and CSB. For CSB, the lower half part of the CSB only is included for the structural analysis model, as shown in Figure 3.1-2. The FE model of RVI assembly is shown in Figure 3.4-1.

Figure 3.4-2 illustrates the CS model. CS consists of a top plate, panels, braces, rings and a bottom plate; these materials are all assembled by welds. The sizes of the weld widths are in the range of 6 to 7 mm. Detailed models with magnified images are provided in Figures 3.4-3 and 3.4-4.

Figures 3.4-5 and 3.4-6 represent the LSS and CSB models, respectively. Figures 3.4-5 and 3.4-6 also show the magnified FE model images of weld areas of LSS and CSB. The size of the LSS weld width is 13.8 mm and CSB welds are 17 mm or 18.5 mm in width. However, insert pins which are supporting the fuel assemblies are not modeled because they don’t need to be evaluated as per EPRI MRP-227-A (Reference 15).

The FE models of the CS, LSS and CSB components are meshed with structural SOLID185 hexahedral elements with 8-nodes.

Since the LSS is assembled with CS and CSB, there are several contacting or welding areas that are modeled using the contact elements. The contacting conditions of those areas are divided into two kinds: contact condition considering weld effect and simple contact condition. One option, a bonded condition, is used to represent the contact condition considering the weld effect and the standard condition option is used for the simple contact condition, to allow a sliding movement between the contact surfaces. Contact points are modeled with the contact elements, CONTA173 and TARGE170, which are a 3-dimensional surface-to-surface contact element and a 3-dimensional target element, respectively. Figures 3.4-7 through 3.4-11 show the FE models of welding or contacting areas among the CS, CSB and LSS components.

3.4.3 Boundary and Initial Conditions

For the structural analyses, symmetry boundary conditions are applied to the symmetric planes of FE quarter model. All nodes at the top of the CSB model are fixed to provide constraint in the vertical direction. Gravitational force (the acceleration of gravity, 9.81 m/sec^2) is applied in the vertical direction in the model. Figure 3.4-12 illustrates the boundary conditions applied and the direction of the acceleration of gravity.

In addition, various loads other than the weight of the RVI components, including the weight, spring force and lifting force of the fuel assemblies, are considered. The initial loads from the fuel assemblies are applied as nodal force to the top of the LSS.

Most parts of the APR1400 RVI are joined by welds that produce residual stresses. Therefore, residual stresses are applied as pre-stress conditions to the welds that are described in Figures 3.4-3 through 3.4-6. An initial component stress (sx, sy, and/or sz) is applied to all welds using USERMAT. The welds of the CS, LSS and CSB reside in different orientations, so it is necessary to allow the proper pre-stress for applied to each weld. Residual stress is assumed to be 379.2 MPa (55 ksi) (Reference 2). The directions of weld residual stress are shown in Figures 3.4-13 through 3.4-16.

3.4.4 Input Data to Structural Analysis (Temperature/Pressure and Neutron Dose)

For the BOC, MOC, EOC and conservative fuel cycle conditions, operating temperatures and pressures are calculated for the RVI components using the CFD code, STAR-CCM+. The calculated results are listed in Tables 3.3-4 through 3.3-7. Neutron dose data inputs are shown in Figures 3.2-8 through 3.2-19. Data in the Tables and Figures contain the additional [ ]^{TS} margin.

3.4.5 Load Sequence

Since the power distribution of the APR1400 does not reach equilibrium until the eighth fuel cycle, a single conservative neutron flux is assumed irrespective of the fuel conditions (BOC, MOC, EOC) and is applied to the first twelve years (which is equivalent to the eighth fuel cycle). The duration of each fuel cycle is 18 months. After the eighth fuel cycle (that is to say, after equilibrium is reached), equilibrium and the best estimated neutron flux and temperature distributions are applied for the remaining thirty-two fuel cycles. For the equilibrium cycles, each cycle consists of the sequential application of temperature distributions and neutron flux for a six-month BOC, six-month MOC and six-month EOC. Figure 3.4-17 presents a schematic diagram of the core loading sequences in the fuel cycles during plant life time. Whenever the fuel cycles start and finish, RVI are heated from and returns to [ ]^{TS} °C. In this calculation, one month is assumed to be 30.5 days.

3.4.6 RVI Materials in Structural Analysis Model

The base materials used in structural analysis model in Section 3.4.2 are identified in Table 3.4-1. They are all Type [ ]^{TS} austenitic stainless steel in annealed condition. For the weld materials, even though they are Type [ ]^{TS} , they are assumed as Type 304 stainless steel.

Table 3.4-1 Material List Used for Structural Analysis Model

TS

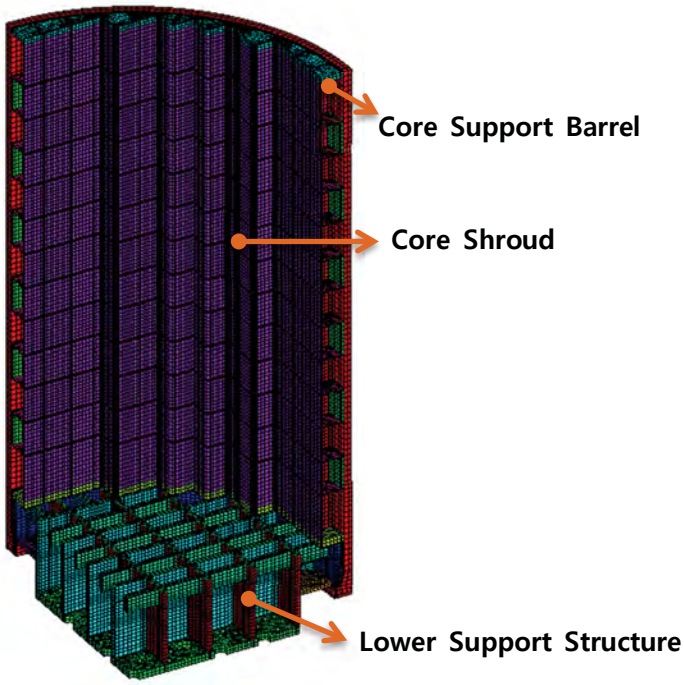

Figure 3.4-1 FE-model of RVI Assembly

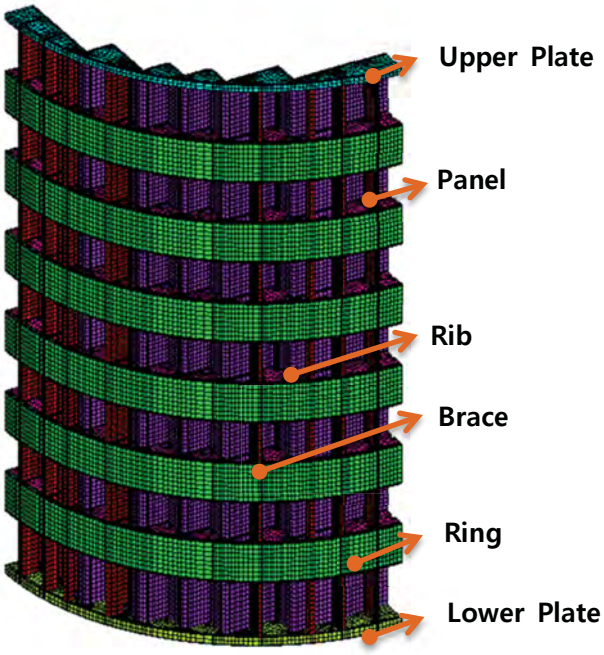

Figure 3.4-2 FE-model of Core Shroud

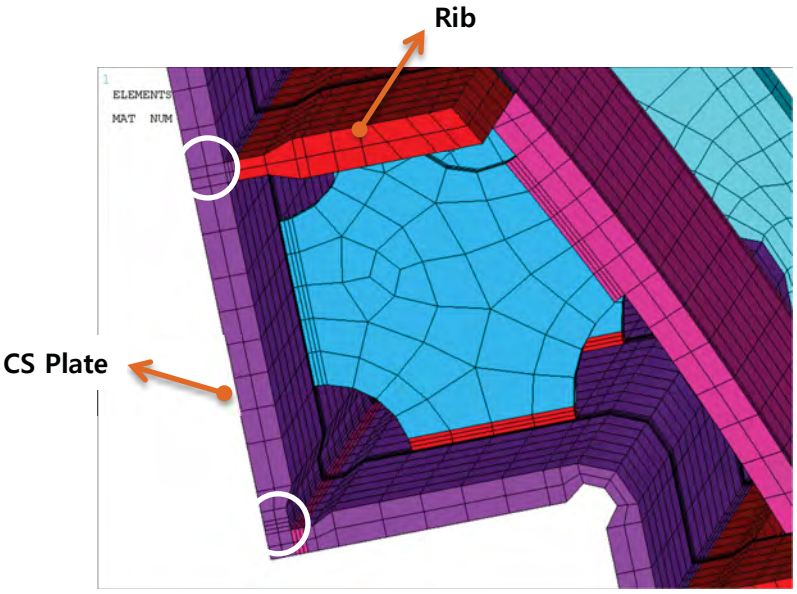

Figure 3.4-3 Welding Areas of Core Shroud(CS Plate-CS Plate & CS Plate-Rib)

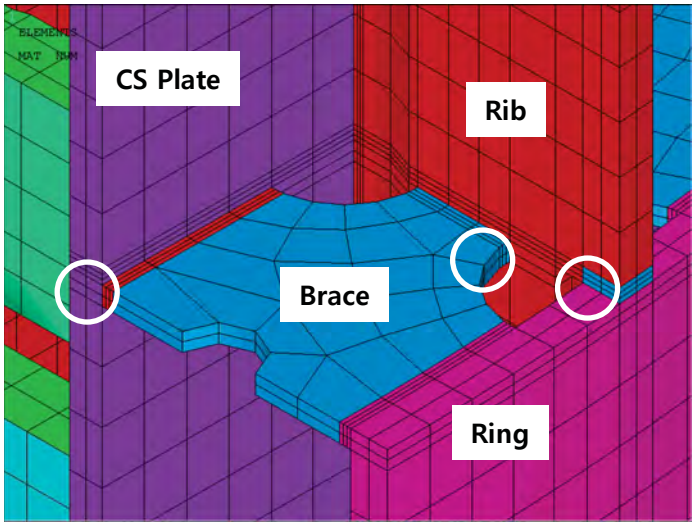

Figure 3.4-4 Welding Areas of Core Shroud(CS Plate-Brace, Brace-Ring and Brace-Rib)

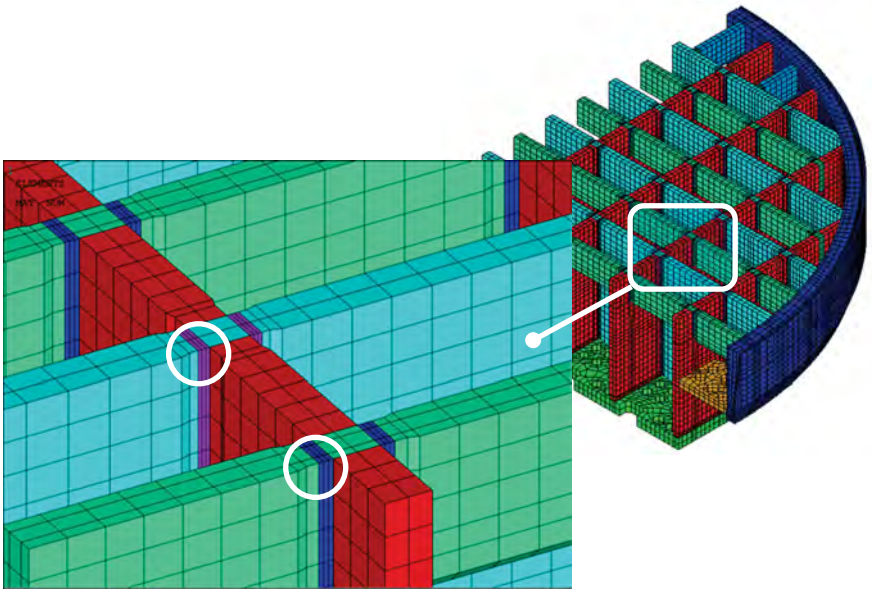

Figure 3.4-5 Welding Areas of Low Support Structure (Main - Secondary Support Beam and Main – Cross Beam)

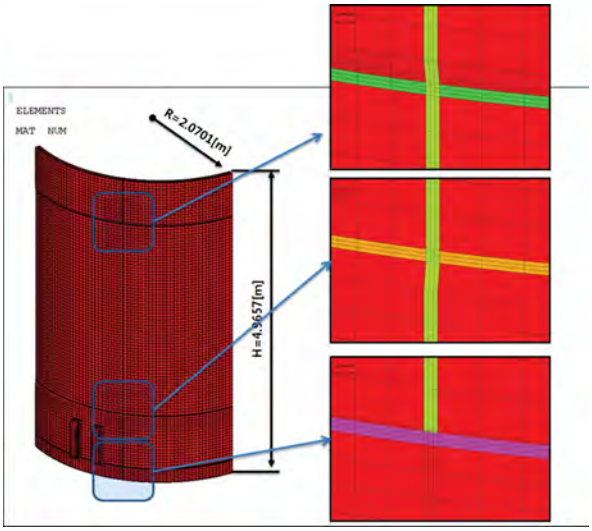

Figure 3.4-6 Welding Areas of Core Support Barrel

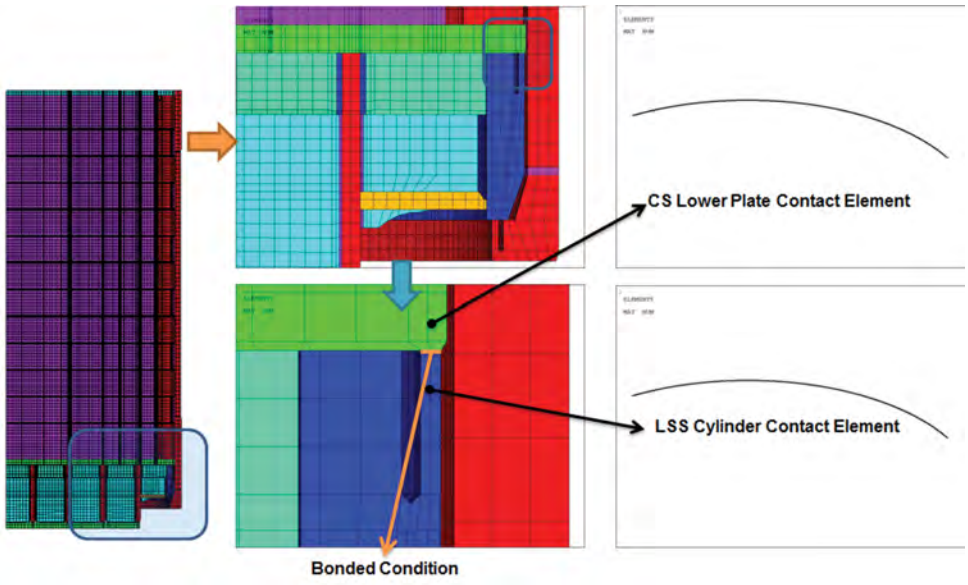

Figure 3.4-7 Welding Area between CS Lower Plate and LSS Cylinder

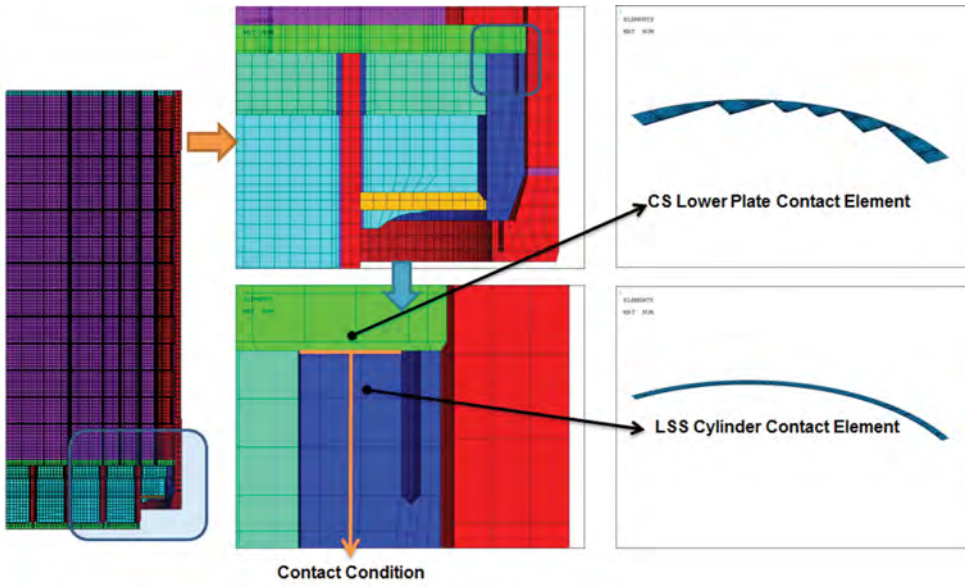

Figure 3.4-8 Welding Area between CS Lower Plate and LSS Cylinder

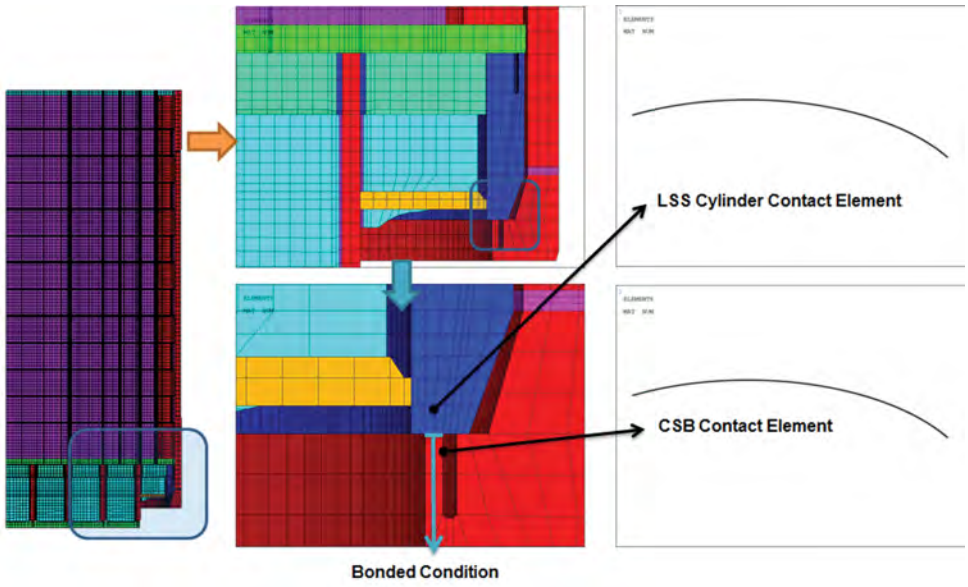

Figure 3.4-9 Welding Area between CSB and LSS Cylinder

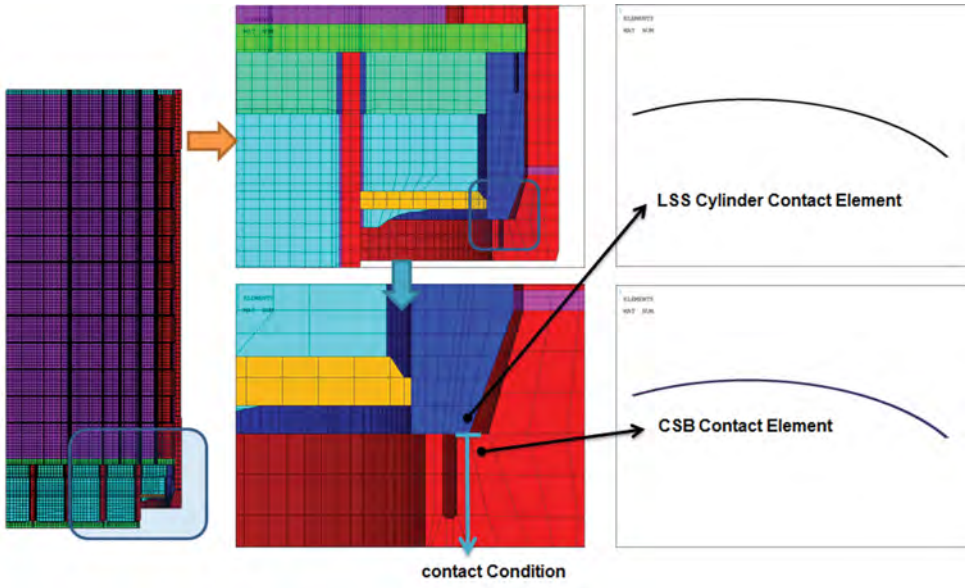

Figure 3.4-10 Contacting Area between CSB -LSS Cylinder

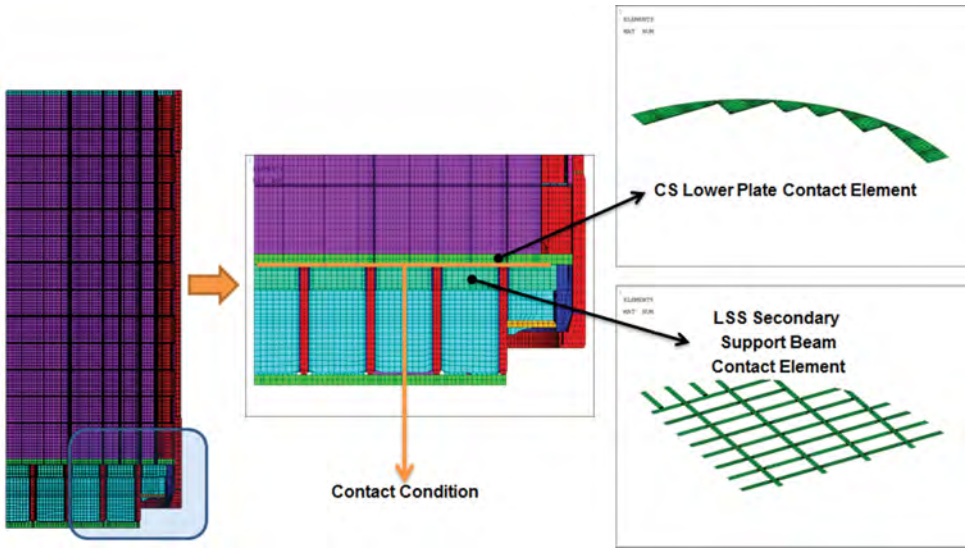

Figure 3.4-11 Contacting Area between CS Lower Plate and LSS

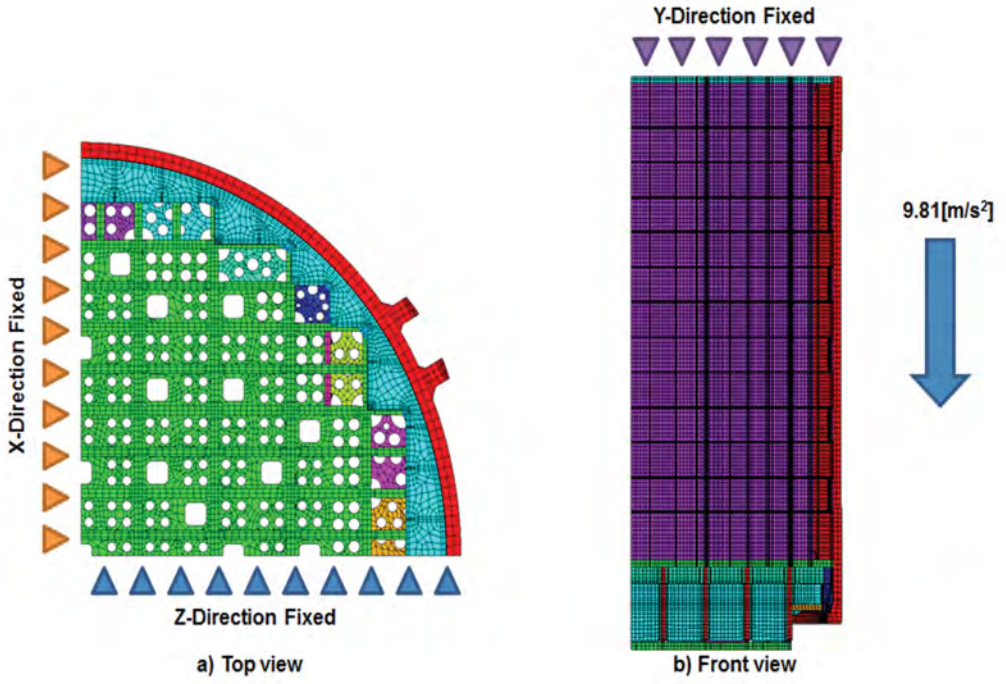

Figure 3.4-12 Boundary and Loading(Gravity) Condition

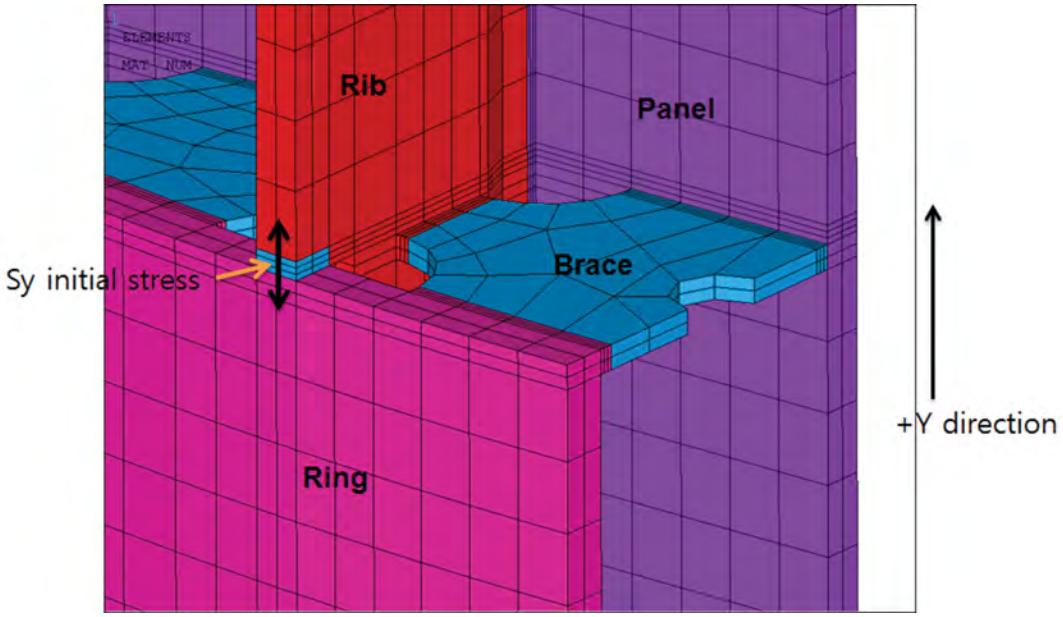

Figure 3.4-13 Weld Pre-stress - Ring & Rib Welds

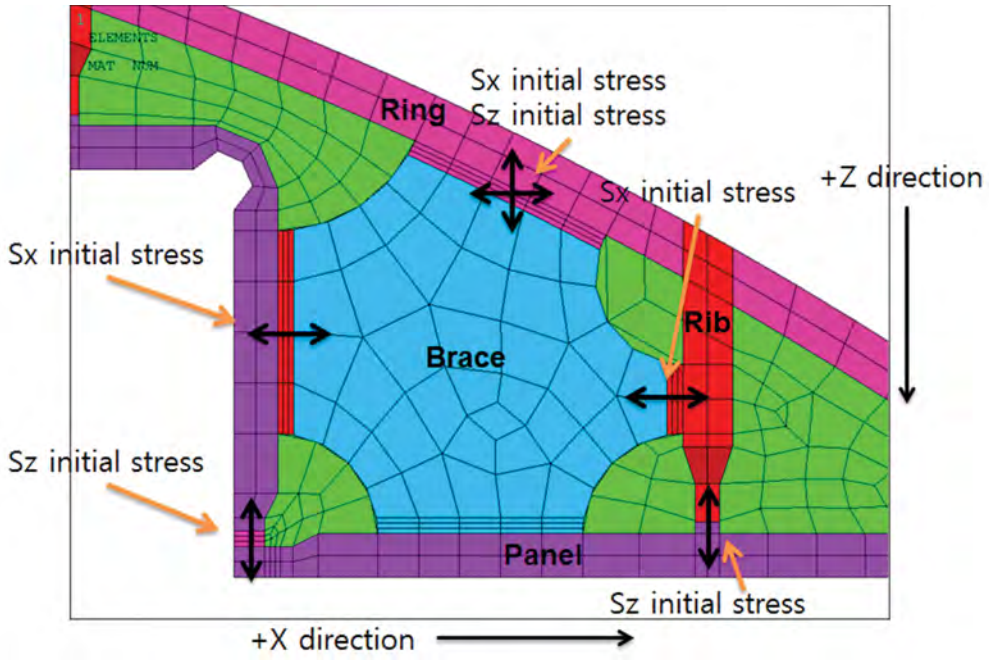

Figure 3.4-14 Weld Pre-stress - Ring Rib, Panel & Brace Welds

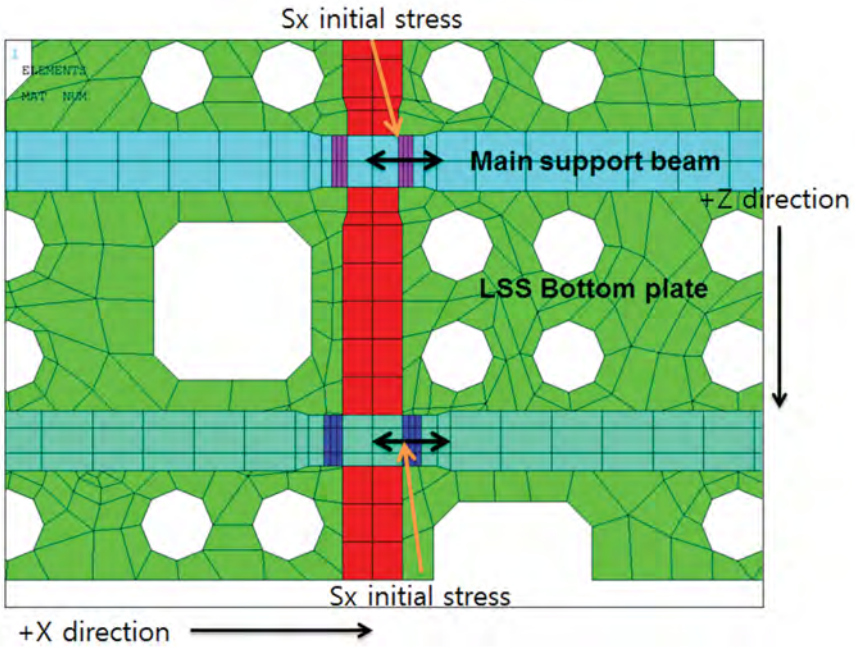

Figure 3.4-15 Weld Pre-stress - Support Beam Welds

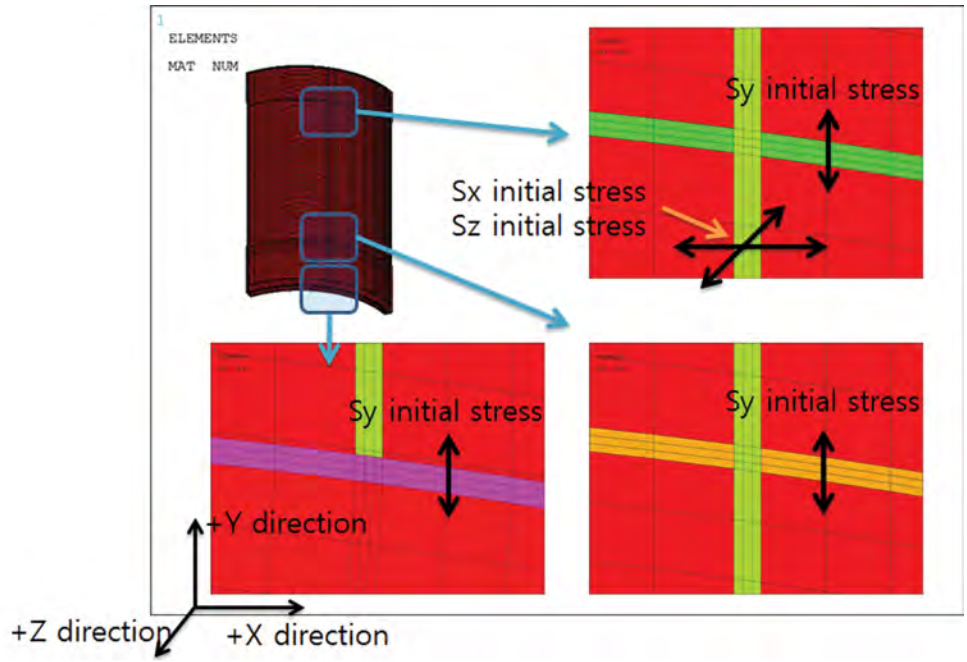

Figure 3.4-16 Weld Pre-stress - CSB Welds

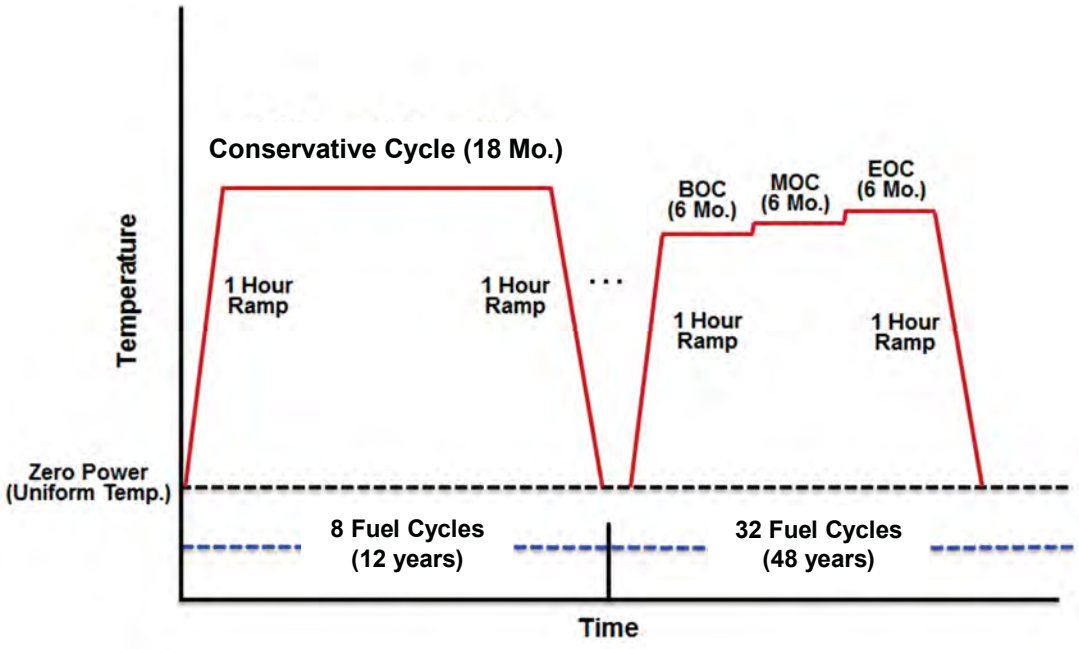

Figure 3.4-17 Load Sequences in Fuel Cycles during Period of 60 Years

4 THE RESULTS OF ANALYSES

4.1 Irradiation Assisted Stress Corrosion Cracking

The IASCC susceptibility ratio is provided by ANSYS/USERMAT state variable 10 (SV 10). This value is calculated by dividing the effective stress by the IASCC susceptibility stress; the results indicate the IASCC susceptibility of irradiated RVI materials. If the value is greater than 1, the corresponding RVI component is assumed to be susceptible to IASCC.

The IASCC susceptibility ratio contour plots at the end of the 60-year operation and time histories are shown in Figures 4.1-1 through 4.1-6 for the CS, LSS, and CSB. Rings do not appear in the Figure 4.1-1 for the clear view. The maximum IASCC susceptibility ratio, [ ]^{TS}, is shown in the weld between the brace and the shroud plate of the CS.

At the area showing the maximum IASCC susceptibility ratio, the IASCC susceptibility ratio remains zero (0) until [ ]^{TS} years of plant operation and increases steeply from [ ]^{TS} years of operation. Then, this value decreases to [ ]^{TS} years of operation and, after that, increases continuously until the end of the 60 year operation period. The first dip or decrease seems to be due to the relaxation of residual stress of the weld. Figure 4.1-7 presents the time history of the effective stress at the maximum IASCC susceptibility ratio point. A similar decreasing trend in the effective stress can be seen between years [ ]^{TS} of operation.

In other areas of the RVI, the IASCC susceptibility ratio is, in general, less than [ ]^{TS}.

Therefore, no propensity to IASCC failure for the APR1400 RVI is expected.

TS

Figure 4.1-1 IASCC Susceptibility Ratio Contour Plot for CS (Maximum Point Is Shown)

TS

Figure 4.1-2 Time History of IASCC Susceptibility Ratio at the Maximum Point in Figure 4.1-1

TS

Figure 4.1-3 IASCC Susceptibility Ratio Contour Plot for LSS (Maximum Point Is Shown)

TS

Figure 4.1-4 Time History of IASCC Susceptibility Ratio at the Maximum Point in Figure 4.1-3

TS

Figure 4.1-5 IASCC Susceptibility Ratio Contour Plot for CSB (Maximum Point Is Shown)

TS

Figure 4.1-6 Time History of IASCC Susceptibility Ratio at the Maximum Point in Figure 4.1-5

Figure 4.1-7 Time History of Effective Stress at the Maximum Point in Figure 4.1-1

4.2 Void Swelling

ANSYS/USERMAT state variable 3 (SV 3) represents irradiation growth strain, which is a linear directional swelling strain due to irradiation and is equal in all three orthogonal directions. Therefore, its unit is mm/mm or in/in. Meanwhile, VS is commonly measured in a volumetric strain (mm^3/mm^3). If it is larger than [ ]^{TS} % for volumetric stain or [ ]^{TS} % for linear strain, the corresponding RVI component is assumed to suffer from VS.

The relationship between the linear irradiation growth strain and volumetric void swelling strain is as follows:

$$\text{Volumetric strain} = (1+ \text{linear strain})^3 - 1 \text{ or}$$

$$\text{Linear strain} = (\text{volumetric strain} + 1)^{1/3} - 1$$

The VS contours at the end of the 60-year operation and their time history are shown in Figures 4.2-1 through 4.2-4 for the CS, LSS and CSB. Rings do not appear in the Figure 4.2-1 for the clear view.

The maximum VS linear strain at the end of 60 year operation is [ ]^{TS} % and this value is larger than the acceptable value of [ ]^{TS} %.

However, if a 93 % capacity factor is considered, the effective full power years will be 55.8 years. Therefore, after a 60 year calendar operation, the maximum VS linear strain is less than [ ]^{TS} % which is smaller enough than the acceptable value of [ ]^{TS} %. Figure 4.2-5 shows the acceptable linear strain as blue colored solid circle and irradiation growth strain at 60 calendar year operation is [ ]^{TS} %.

Therefore, no propensity to VS failure for APR1400 RVI is expected.

Figure 4.2-1 VS Linear Strain Contour Plot for CS (Maximum Point Is Shown)

Figure 4.2-2 Time History of VS Linear Strain at the Maximum Point in Figure 4.2-1

Figure 4.2-3 VS Linear Strain Contour Plot for LSS (Maximum Point Is Shown)

Figure 4.2-4 VS Linear Strain Contour Plot for CSB (Maximum Point Is Shown)

TS

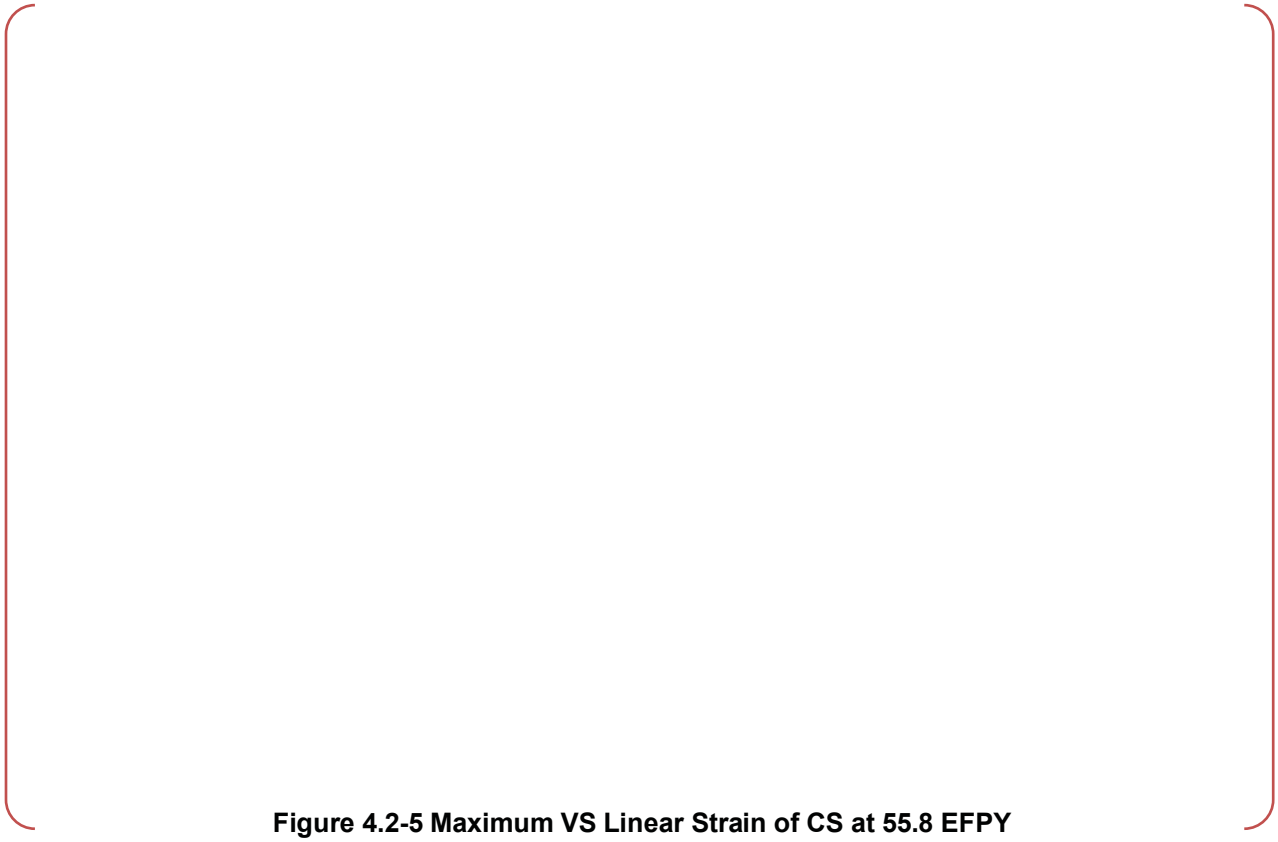

Figure 4.2-5 Maximum VS Linear Strain of CS at 55.8 EFPY

5 CONCLUSIONS

APR1400 RVI components are operated for a 60 calendar year design life under the environment of the operating temperature, pressure and neutron or gamma irradiation. All components of the RVI, whose materials are considered as annealed austenitic stainless steels, were evaluated for IASCC and VS, which are challenging degradation mechanisms affecting the integrity of the RVI. Best estimate but still conservative analyses were performed for the CS, LSS and the lower half part of the CSB. The analyses consist of irradiation transport analysis, CFD analysis and structural analysis. Steady-state operating conditions are assumed for these analyses. Other normal or upset transients are not considered because they are not related to degradations such as IASCC and VS.

Neutron fluxes and heat sources were calculated for BOC, MOC and EOC of fuel assemblies for the equilibrium fuel cycles and for conservative fuel cycles assuming a conservative radial pin power distribution and axial power shape irrespective of BOC, MOC or EOC. A low leakage core is assumed in this analysis. MCNP code, version 5 was used.

The CFD analysis calculated, through conjugate heat transfer analysis coupled with an analysis of coolant flow, the temperature and pressure distributions on the surfaces of the RVI components using neutron fluxes and heat sources as inputs for equilibrium fuel cycles including BOC, MOC and EOC, and for conservative fuel cycles. STAR-CCM+ was used.

ANSYS code equipped with USERMAT was used to provide information on the IASCC susceptibility ratio (state variable 10) and VS irradiation growth strain (state variable 3). Structural analysis was performed according to the loading sequences for the initial 8 conservative fuel cycles (12 year operation) and remaining 48 year equilibrium fuel cycle operation.

IASCC susceptibility ratio is represented by ANSYS/USERMAT state variable 10 (SVAR10). The maximum IASCC ratio, [ ]^{TS}, occurs at the one of welds between the brace and the shroud plate of the CS, however, in other areas it is in general less than [ ]^{TS}.

ANSYS/USERMAT state variable 3 (SVAR3) represents irradiation growth strain, which is a linear directional swelling strain due to irradiation and is equal in all three orthogonal directions. The maximum VS linear strain at the end of 60 year operation is [ ]^{TS} % at the shroud plate of the CS; this value is larger than the acceptable value of [ ]^{TS} %. However, if a 93% capacity factor is considered, the maximum VS linear strain is less than [ ]^{TS} %, which is smaller enough than the acceptable value of [ ]^{TS} %.

Therefore, the APR1400 RVI components are not expected to suffer from IASCC and VS degradations during the 60 year design life.

6 REFERENCES

(1) APR1400 Design Control Document Tier 2, KHNP, APR1400-K-X-FS-14002, Rev. 0, Dec. 2014.

(2) Materials Reliability Program: PWR Internals Material Aging Degradation Mechanism Screening and Threshold Values (MRP-175), EPRI, Palo Alto, CA: 2005. 1012081.Materials Reliability Program: Functionality Analysis for Westinghouse and Combustion Engineering Representative PWR Internals (MRP-230, Revision 2), EPRI, Palo Alto, CA: 2012. 1021026.

(3) Materials Reliability Program: Functionality Analysis for Babcock & Wilcox Representative PWR Internals (MRP-229-Rev. 3), EPRI, Palo Alto, CA: 2010. 1022402.

(4) Materials Reliability Program: Aging Management Strategies for B&W Pressurized Water Reactor Internals (MRP-231-Rev. 2), EPRI, Palo Alto, CA: 2010. 1021028.

(5) Materials Reliability Program: Aging Management Strategies for Westinghouse and Combustion Engineering PWR Internal Components (MRP-232, Revision 1), EPRI, Palo Alto, CA: 2012. 1021029.

(6) ASME Boiler and Pressure Vessel Code, 2007 Edition with 2008 Addenda.

(7) CCC-650/DOORS3.2a, “One-, Two-, and Three Dimensional Discrete Ordinates Neutron/Photon Transport Code System,” Radiation Safety Information Computational Center, Oak Ridge National Laboratory, Oct. 2003.

(8) ANSYS 14.5, User’s Manual, ANSYS, Inc.

(9) ANATECH Report, No. ANA-05-R-0684 Rev. 3.12, “Installation and User’s Manual for Version 3.12 of Constitutive Model for Irradiated Austenitic Stainless Steels for Use with ANSYS”, April, 2010.

(10) “MCNP – A General Monte Carlo N-Particle Transport Code Version 5”, Los Alamos National Laboratory Vols. I-III, April 2003.

(11) M. B. Chadwick, et al, “ENDF/B-VII.1 Nuclear Data for Science and Technology: Cross Sections, Covariances, Fission Product Yields and Decay Data,” "Brookhaven National Laboratory, 2011.

(12) M. C. White, "Photoatomic Data Library MCPLIB04: A New Photoatomic Library Based on Data from ENDF/B-VI Release 8,”" Los Alamos National Laboratory internal memorandum X-5:MCW-02-111 (2002).

(13) STAR-CCM+ version 8, User’s Manual, CD-Adapco.

(14) Material Reliability Program: Development of Material Constitutive Model for Irradiated Austenitic Stainless Steels (MRP-135-Rev. 1), EPRI, Palo Alto, CA: 2010. 1020958.

(15) Material Reliability Program: Pressurized Water Reactor Internals Inspection and Evaluation Guidelines (MRP-227-A, EPRI, Palo Alto, CA: 2012. 1022863